SCALE UP SOLUTIONS FOR LIQUID BASED MICROFLUIDIC FUEL CELL

By

Bernard Ho

B. Sc., University of Victoria, 2007

THESIS SUBMITTED IN PARTIAL FULFILLMENT OF
THE REQUIREMENTS FOR THE DEGREE OF

MASTER OF APPLIED SCIENCE

In the

School of Engineering Science

Mechatronic Systems Engineering

SIMON FRASER UNIVERSITY

Summer 2012

APPROVAL

Name: **Bernard Ho**

Degree: **Master of Applied Science**

Title of Thesis: **Scale up Solutions for Liquid Based Microfluidic Fuel Cell**

Examining Committee:

Chair: **Dr. Krishna Vijayaraghavan**
Assistant Professor of Engineering Science

Dr. Erik Kjeang
Senior Supervisor
Assistant Professor of Engineering Science

Dr. Edward Park
Supervisor
Associate Professor of Engineering Science

Dr. Gary Wang
Supervisor
Professor of Engineering Science

Dr. Martin Ordonez
Internal Examiner
Assistant Professor of Engineering Science

Date Defended/Approved: July 4th, 2012

Partial Copyright Licence

ABSTRACT

A microfluidic fuel cell is a microfabricated device that produces electrical power through electrochemical reactions involving a fuel and an oxidant. In this study, vanadium redox electrolytes will be used as reactants. Microfluidic fuel cell systems exploit co-laminar flow on the microscale to separate the fuel and oxidant species, in contrast to conventional fuel cells employing an ion exchange membrane for this function. In order to maintain this regime specific to microscale, the size of the device is limited, which directly impacts the power output. In this study, scale up methods are investigated. In order to keep the microfluidic co-laminar flow regime, flow distribution over the whole active area is the main challenge. Two approaches have been investigated: a multiplexing approach and a dimensional scale up approach. For both solutions, prototypes have been designed, built, tested with Vanadium electrolytes as reactants, and compared with the performance of a unit cell. With the multiplexing approach, we managed to get performance on par with the unit cell, with the dimensional scale up, we managed to have a total power output of 130mW, the highest power output reported yet for microfluidic fuel cells.

Keywords: Vanadium, Microfluidic, Microfuelcell, Scale up, Membraneless

ACKNOWLEDGEMENTS

I would like to thank my supervisor, Dr. Erik Kjeang, for his guidance, support and inspiration during my graduate studies, all my teammates, Jinwook Lee, Abhishek Nanjundappa, Xiaoye Liang, Deepak Krishnamurthy, Larry Hoang, Peter Hsiao, Jun Hong, Marius Haidicu.

I would also like to thank Dr. Edward Park. Dr. Gary Wang, Dr. Martin Ordonez and Dr. Krishna Vijayaraghavan for reviewing this thesis.

On a more personal note, I would like to thank Cécile Mancuso for her day to day support over these years, and Claire for her support towards the very end of my work that was crucial.

TABLE OF CONTENTS

LIST OF FIGURES

NOMENCLATURE

F	Faraday's constant (C mol^{-1})
I	electrical current (Amp)
$\dot{m}$	mass flow rate (kgs^{-1})
P	pressure, (Pa)
PEM	Polymer Electrolyte Membrane
AAEM	Alkaline Anion Exchange Membranes
PMMA	Poly(methyl methacrylate)
PDMS	Polydimethylsiloxane
V	output voltage (V)
W	power (W)
GDL	Gas Diffusion Layer
GDE	Gas Diffusion Electrode
OCV	Open Circuit Voltage
V(II)	Vanadium 2 (V^{2+})
V(III)	Vanadium 3 (V^{3+})
V(IV)	Vanadium 4 (VO^{2+})
V(V)	Vanadium 5 (VO_2^{+})

Greek symbols

μ	fluid viscosity ($N.s.m^{-2}$)
ν	kinematic viscosity ($m^2\ s^{-1}$)
ρ	density ($kg\ m^{-3}$)

1. INTRODUCTION

1.1 Microfluidic fuel cell vs. conventional fuel cell

A fuel cell [1] is an energy conversion device that converts chemical energy stored in a fuel and oxidant into electrical energy through an electrochemical process involving oxidation-reduction reactions. Contrary to the battery, the fuel cell is continuously fed with reactants, i.e., a fuel and an oxidant. The oxidation and reduction reactions take place at the anode and cathode, respectively, and together form an electrochemical cell reaction. The anode and cathode have to be ionically connected to each other with a material that conducts ionic charge carriers such as protons or hydroxide ions while blocking undesired transport of reactants and electric current. Proton Exchange Membranes (PEM) or Alkaline Anion Exchange Membranes (AAEM) developed to fulfill that function composes the centre of the fuel cell flanked by one electrode (anode and cathode) on each side, as illustrated in Figure 1.

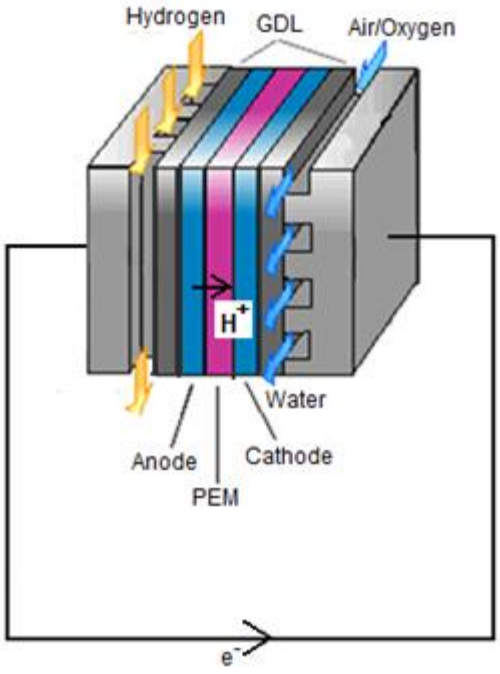

Figure 1: Schematic of a hydrogen PEM fuel cell [2].

The membrane is coated with a catalyst layer on each side that enhances the electrochemical reactions and is sandwiched between two Gas Diffusion Layers (GDL) that provide mechanical support to the membrane, electrical conduction to the current collectors, and reactant and product transport to and from the active sites in the catalyst layers. Most fuel cells developed to date run on hydrogen, methanol, or formic acid as fuel and oxygen from the surrounding air as oxidant.

Compared to batteries, fuel cells offer the benefits of instant recharge by adding fresh reactants from a cartridge for instance, and higher energy density depending on the selection of fuel. Fuel cells have wide application ranges from microelectronics applications to several kilowatts backup power units and can even be used in the automotive industry for cars and buses with electric powertrains. Most fuel cells produce clean electric power without generation of greenhouse gases or any other harmful emissions. For instance, the hydrogen PEM fuel cell, one of the most common fuel cells available on the market, produces no emissions other than pure water. The main challenges presently facing the fuel cell industry are related to cost and durability. The durability (or lifetime) of the fuel cell is often limited by membrane degradation due to chemical and physical damage occurring during cyclic operation. The membrane also needs to be hydrated to provide adequate ionic conductivity, which requires complex water management systems or limits the operational range. Excessive hydration on the other hand generates a flooding effect that prevents reactants to reach the active sites. In addition, the catalyst layer suffers migration and agglomeration issues at a molecular level, which significantly decreases the surface area and hence its performance over time [3]. Perhaps more importantly, the cost of both membrane and catalyst layers is relatively high. Of particular concern is the cost of platinum, a precious metal with very limited supply required to promote the electrochemical reactions involving hydrogen and oxygen.

Microfluidic fuel cell systems provide an opportunity to overcome the challenges associated with the use of PEM or AAEM membranes in conventional fuel cells. Microfluidic fuel cell technology [4] eliminates the need of a membrane by utilizing laminar flow on the microscale in three main configurations: (i) a single stream of flowing electrolyte; (ii) two parallel streams of fuel and electrolyte or fuel and oxidant

flowing in a stratified, co-laminar format; and (iii) three parallel streams of fuel, electrolyte, and oxidant in a similar co-laminar format. The former configuration, which replaces the membrane with an electrolyte stream in a thin microchannel, is well-suited for cells using gaseous reactants such as hydrogen and oxygen/air distributed in separate flow channels. The latter two configurations operate based on co-laminar flow of two or more liquid phase streams running at low Reynolds numbers, where all turbulent or convective sources of detrimental cross-stream mixing are eliminated. Each stream contains electrolyte that facilitates ionic charge conduction between the electrodes while the fuel and oxidant species are carried in separate streams. The rate of cross-stream diffusion between the fuel and oxidant streams is relatively slow and can be actively controlled by adjusting the flow rate of each stream or by introducing a third electrolyte stream. Microfluidic fuel cells can be designed and built using inexpensive microfabrication and micromachining methods, e.g., photolithography, soft lithography, and laser etching, compatible with high volume manufacturing.

Using more concentrated chemicals or chemicals that have faster kinetics can solve the need of having a catalyst. Microbial species can also be used as catalysts in biofuelcells (using bacteria or enzymes). However, biofuelcells [5, 6, 7] have a short lifetime associated with the life expectancy of such living cells, and low power output. Addressing those major issues makes microfluidic fuel cell very simple to fabricate and run, but also very inexpensive.

1.2 Review of microfluidic fuel cells

Research and development in the area of microfluidic fuel cells has accelerated over the past few years. The detailed study by Kjeang et al. [4], highlighting relevant microfluidic fuel cell contributions reported prior to 2008, is a comprehensive resource in this field. Another review written by myself and Dr Kjeang [8], part of which is included in this section, highlights the contributions after 2008 and provides a novel classification scheme for microfluidic fuel cells based on the fluidic phases of the fuel and oxidant streams. The following three microfluidic fuel cell categories are defined: (i) gaseous fuel and oxidant [9, 10]; (ii) liquid fuel and gaseous oxidant [11, 12, 13, 14]; and (iii) liquid fuel and oxidant [15, 16].

1.2.1 Microfluidic fuel cells with gaseous fuel and oxidant

The microfluidic fuel cell category with gaseous fuel and oxidant is dominated by alkaline electrolyte fuel cells running on hydrogen and oxygen. Alkaline fuel cells are based on anion exchange during the electrochemical cell reaction, instead of proton exchange for conventional acidic media fuel cells. The anode and cathode reactions are:

$$H_2 + 2\,OH^- \rightarrow 2\,H_2O + 2\,e^- \;(Anode\ side)$$

$$O_2 + 2\;H_2O + 4\,e^- \rightarrow 4OH^- \;(Cathode\ side)$$

Compared to its acidic media counterpart, the alkaline based hydrogen fuel cell is known to be more cost-effective as many transition metals are more stable in an alkaline environment, allowing the use of non-precious based metals as catalysts. Moreover, the oxygen reaction (which is the limiting reaction in the acidic media fuel cell) has superior kinetics in alkaline media [10, 17, 18]. Alkaline hydrogen/oxygen fuel cells were successfully developed for the Apollo space program in the 1960s [19] used separate on-board storage tanks of compressed hydrogen and oxygen, and found their main use in air-free or air-limited environments.

The main challenge in alkaline based fuel cells that use air as oxidant and/or hydrocarbon fuels is carbonate formation from CO_2 that depletes the hydroxide ions from the electrolyte via the following reaction:

$$CO_2 + 2\,OH^- \rightarrow H_2O + CO_3^{2-}\,(Electrolyte)$$

Carbonate species precipitate in the electrode and membrane structure, blocking electrode active sites and membrane pores and retarding reactant transport, while also reducing the electrolyte conductivity by consuming hydroxide ions. More recently, through many scientific breakthroughs in the area of microsystems and microtechnologies, innovative microfluidic fuel cell systems have emerged as an alternative solution which demonstrated the ability to remove carbonate precipitates from the active site surface by adding an electrolyte microflow [9, 10].

In the alkaline microfluidic fuel cell architecture shown in Figure 2, gaseous hydrogen and air are used as fuel and oxidant, similarly to conventional acidic media hydrogen fuel cells. The microfluidic feature of this fuel cell system is the electrolyte microchannel, where a liquid electrolyte microfluidic stream is employed in place of a membrane.

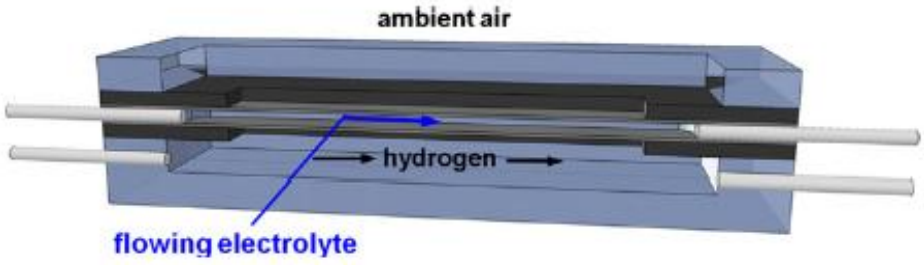

Figure 2: Alkaline microfluidic fuel cell system with gaseous hydrogen and air reactants [10]. Copyright Elsevier (2011).

The electrolyte is flowing in a laminar regime at low Reynolds numbers due to the microscale channel dimension, in between two liquid-impermeable hydrophobic gas diffusion electrode (GDE) layers, exposed to hydrogen and air on the opposite sides. A proof-of-concept device was recently demonstrated that produced up to 300 mA cm^{-2} current density and 47 mW cm^{-2} power density at room temperature [10]. A parametric

study was performed to investigate the effect of electrolyte concentration and flow rate along with catalysts and PTFE content on performance, lifetime, and carbonate formation sensitivity. It was shown that increased electrolyte concentration has a positive impact on performance up to a KOH concentration range between 3M and 5M, as a result of improved ionic conductivity and reduced ohmic losses in the cell. At higher concentrations, the performance decreased. This tendency may be attributed to a higher viscosity of the electrolyte [20], which resulted in anode flooding. The excess K^+ ions may also produce a shielding effect on the anode side and the high hydroxide concentration can monopolize all the reaction sites, thus making it more difficult for hydrogen adsorption to occur [21].

For GDE design improvements, PTFE content is important as a binder and to obtain hydrophobicity properties, avoiding flooding. An optimum PTFE content of 40% is reported in the literature, which is confirmed by recent experiments [9]. A gradually increasing performance trend is found over the first few reported cell architectures. The latest prototypes achieved peak power density levels up to 108 mW cm^{-2} using pure oxygen and platinum catalyst and 68 mW cm^{-2} using silver catalyst. As can be expected, the performance obtained with air-breathing systems is lower with peak values of 47 mW cm^{-2}.

1.2.2 Microfluidic fuel cells with liquid fuel and gaseous oxidant

Microfluidic fuel cells with liquid fuel and gaseous oxidant are dominated by methanol and formic acid fuels in combination with air as oxidant. As illustrated by the schematic in Figure 3, the liquid phase fuel stream is paired with a second liquid stream of blank electrolyte required to separate the fuel stream from the cathode active sites which would otherwise lead to severe crossover effects. Methanol and formic acid are available as highly concentrated liquids and are therefore favourable for applications requiring high energy densities, e.g., portable electronic equipment. Both acidic and alkaline electrolyte compositions have been reported for liquid/gaseous microfluidic fuel cell systems. The reaction schemes are as follows:

Methanol in acidic media:

$$CH_3OH + H_2O \rightarrow 6H^+ + 6\,e^- + CO_2\ (Anode\ side)$$

$$\frac{3}{2}O_2 + 6H^+ + 6\,e^- \rightarrow 3H_2O\ (Cathode\ side)$$

Methanol in alkaline media:

$$CH_3OH + 6OH^- \rightarrow 5H_2O + 6\,e^- + CO_2\ (Anode\ side)$$

$$\frac{3}{2}O_2 + 3H_2O + 6\,e^- \rightarrow 6OH^-\ (Cathode\ side)$$

Formic acid in acidic media:

$$HCOOH \rightarrow 2H^+ + 2\,e^- + CO_2\ (Anode\ side)$$

$$\frac{1}{2}O_2 + 2H^+ + 2\,e^- \rightarrow H_2O\ (Cathode\ side)$$

Formic acid in alkaline media:

$$HCOO^- + 3OH^- \rightarrow 2H_2O + 2\,e^- + CO_3^{2-}\ (Anode\ side)$$

$$\frac{1}{2}O_2 + H_2O + 2\,e^- \rightarrow 2OH^-\ (Cathode\ side)$$

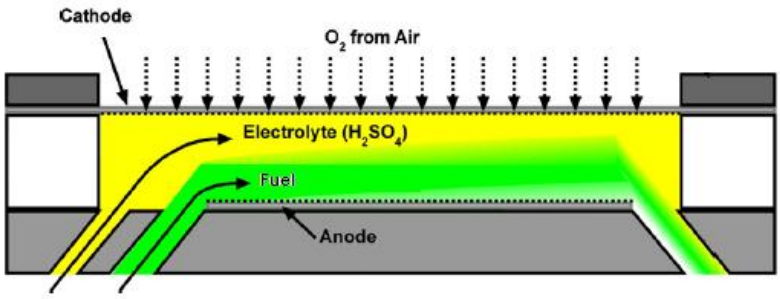

Figure 3: Microfluidic air-breathing direct methanol and formic acid fuel cell system design [14]. Copyright Elsevier (2009).

The first generation of microfluidic direct methanol and formic acid fuel cells featured a liquid/liquid configuration with dissolved oxygen in an aqueous media as the oxidant. Because of their low performance, principally due to the low solubility and diffusivity of oxygen in aqueous media, other solutions were investigated, e.g., using a concentrated liquid oxidant like hydrogen peroxide [22], hypochlorite [23], nitric acid [24], or designing an air-breathing microfluidic fuel cell system [25, 26].

Overall, for air-breathing microfluidic direct methanol and formic acid fuel cells, crossover remains one of the main challenges, as the fuel concentrations are relatively high and recirculation of unused fuel may be required from a system efficiency standpoint. To address this issue, research on selective catalysts [11, 12, 14] and nanoporous separators [13] show promising advancements.

By adding a nanoporous separator between the electrolyte and fuel streams made of 6 μm polycarbonate with $6x10^8$ holes per cm² with a diameter of 0.05 μm, the crossover diffusion rates were significantly reduced. The cell performance increased from 28 mW cm^{-2} for a conventional methanol microfluidic fuel cell to more than 40 mW cm^{-2} with the nanoporous separator and up to 70 mW cm^{-2} when a thin Nafion layer was added on the cathode GDE (using 1M methanol as fuel). Further crossover reductions can be achieved through reduction of methanol concentration, which would decrease performance but increase fuel utilization [13].

Research on catalyst selectivity is another way to resolve crossover issues. Ruthenium selenium chalcogenides, for instance, are relatively insensitive to methanol [11] in relation to platinum which is largely affected by mixed potential losses due to methanol

crossover. For microfluidic methanol fuel cells tested with Ru-Se anodes, the performance was independent of crossover even at high fuel concentrations. Similar experiments were also performed on microfluidic formic acid fuel cell systems with consistent trends [12, 14].

Methanol and formic acid based fuel cell systems generate carbon dioxide as a product of the electrochemical oxidation. CO_2 bubbles are generally not observed due to high solubility in water at room temperature and low reaction rates, but gas bubbles will likely become an issue for microfluidic fuel cells operating at higher current densities. Gas bubbles have a crucial impact on the cell performance as it may disturb the stability of the co-laminar flow and the ionic exchange occurring through the electrolyte [27].

The channel geometry also has an important effect on diffusion, hence crossover. It also affects pressure within the microfluidic fuel cell which has an impact on bubble formation, closely linked to the CO_2 solubility in liquids. Straight, converging, and diverging channels were tested [28], and it was shown that a diverging channel design enhances diffusion and bubble formation.

1.2.3 Microfluidic fuel cells with liquid fuel and oxidant

Microfluidic fuel cells with both fuel and oxidant present in the liquid phase generally utilize two co-laminar microfluidic streams, one carrying the fuel and the other carrying the oxidant, in a shared microfluidic channel without a membrane or any other physical separation between the streams. Historically, this is the most frequently published type of microfluidic fuel cell [4] due to the simplicity of the co-laminar flow. Cells utilizing a variety of fuels and oxidants have been reported, including formic acid, methanol, dissolved hydrogen, dissolved oxygen, and hydrogen peroxide, as detailed elsewhere [4]. The American company Laminare Technologies is commercially developing liquid based microfluidic fuel cells using dissolved hydrogen in alkaline supporting electrolyte as fuel and dissolved oxygen as oxidant in acidic supporting electrolyte. Laminare's patented microfluidic fuel cell technology, originating at Cornell University [29], employs a strategically patterned substrate to induce secondary motion and enhance mass transport rates in the microchannel [30].

Albeit the benefits attributed to this technology are proven, the performance of microfluidic fuel cells using dissolved gases (e.g., oxygen) in the liquid phase is considerably constrained by the low solubility and consequently low concentration of the dissolved species [4]. Three main approaches that enhance the performance of liquid/liquid microfluidic fuel cells with dissolved gases have recently been demonstrated: (i) using alkaline and acidic electrolytes in the anodic and cathodic streams, respectively, to boost the electrochemical cell potential (more negative anode and more positive cathode potentials, thus increasing the cell potential), as adopted by Laminare's fuel cell system as previously described, ; (ii) investigating better catalysts that have a lower sensitivity to crossover, as previously discussed [11-14]; and (iii) finding alternative oxidants and membrane architectures to limit the crossover. Neah Power Systems, a US company developing liquid/liquid microfluidic fuel cells, recently presented a unique cell design utilizing a flow-through porous silicon anode and a flow-by porous silicon cathode [31].This patented fuel cell architecture [24] is compatible with methanol and formic acid as fuel on the anode side, and uses moderately concentrated nitric acid as oxidant on the cathode side:

$$3HNO_3 + 6H^+ + 6\,e^- \rightarrow 3HNO_2 + 3H_2O\ (Cathode\ side)$$

Sulfuric acid was added to improve the proton conductivity of the solutions. The electrodes were micro-machined in silicon and coated with catalyst. The cathode was coated with an ink barrier in a subsequent step to prevent mixing of the two streams. The performance obtained for this fuel cell reached relatively high levels, up to 200 mW cm^{-2} at 60°C, depending on the concentration of the species and the operating temperature. However, this cell suffered from crossover issues and performance degradation as unused fuel and oxidant were recirculated during operation.

1.2.4 Architectures and comparison of vanadium based microfluidic fuel cells:

Vanadium redox electrolyte, developed commercially for vanadium redox battery technology, provides an all-liquid reactant pair available at high concentrations that is well-suited for microfluidic fuel cell systems. The vanadium redox species are dissolved in dilute sulfuric acid which acts as supporting electrolyte. The electrochemical reactions are based on the following vanadium redox scheme:

$$V^{2+} \rightarrow V^{3+} + e^-\ (Anode\ side)$$

$$VO_2^+ + 2H^+ + e^- \rightarrow VO^{2+} + H_2O\ (Cathode\ side)$$

Microfluidic vanadium fuel cells do not require any catalyst, as the kinetics of the aforementioned electrochemical reactions is rapid on plain carbon. Preliminary microfluidic vanadium fuel cell devices employed a flow-over configuration with co-laminar flow in a high-aspect ratio microchannel over carbon electrodes located on the bottom wall, consisting of sputtered graphite on gold [32], graphite rods [33], and porous carbon paper [34]. More recently, a microfluidic vanadium fuel cell with flow-through porous carbon electrodes was demonstrated [35].

Different architectures shown in Figure 4 were invented, each one with its own specific characteristics, depending on the fuel and oxidant used, and the electrode design: X [15], F, Y [32] or T [35] shaped channels were used. For electrodes and current collectors that

are relatively non porous, F and Y shaped channel designs were adopted. The reactants are flowing along the surface of the electrodes. More efficient designs emerged a few years after with the concept of "flow through" electrodes. Using porous electrodes such as carbon paper made of carbon fibres significantly increase the performance of such fuel cells as more surface area is available for the chemical reactions to take place.

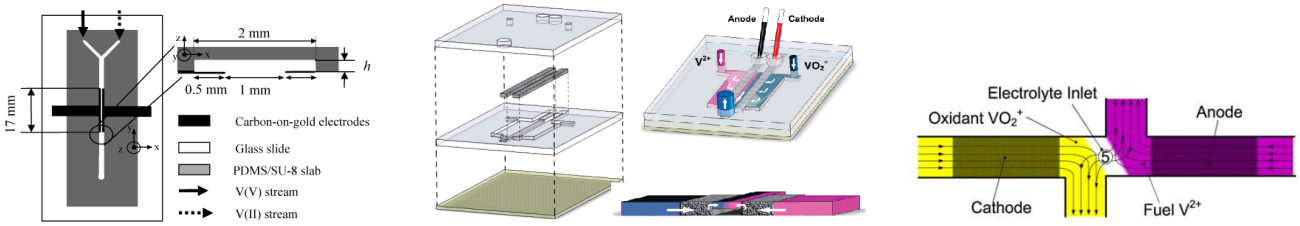

Ferrigno et al. design [32] Kjeang et al. design [35] Salloum et al. design [15]

Figure 4: Architecture comparison.

Copyright 2002 and 2008 American Chemical Society. Copyright Elsevier (2010).

Ferrigno et al. [32] can be considered to be the first to develop microfluidic vanadium fuel cell. The initial flow field design was a relatively simple Y shape design fabricated using microfabrication techniques (soft lithography), with straight flow over graphite electrodes where the vanadium species used for fuel and oxidant are flowing along the electrodes. This fuel cell didn't require any catalyst, but the fuel utilization was very low (from 1 to 5% of the reactants used). The performance was relatively low as well, achieving a power density of 38mW/cm², but considering that neither membrane nor catalysts were used, the first step in this field was promising.

A few years later, Kjeang et al. [35] created a new design based on this technology with significant performance improvements. The flow field was a relatively simple T shape design, but porous carbon electrodes (Toray carbon fibre paper) were used this time instead of graphite, in a parallel design with the waste channel. The use of porous carbon fibre paper considerably increases the contact surface area which greatly improves the kinetics of the electrochemical reactions and hence, fuel utilization (up to 94% after one

pass). The power density achieving 131mW/cm² was significantly improved from the previous flow over design of Ferrigno et al. [32].

The fuel and oxidant react inside the electrodes with a distinct color change before and after the electrode. This design also open a new door: being able to run the fuel cell as an electrolyser in order to recycle the waste using the same device, but such a thing can only be achieved if the fuel utilization is high enough to recycle the fuel in one pass to avoid contaminating the initial fuel and oxidant reservoirs. The fabrication method has also been improved by using plasma treatment to bond the patterned PDMS on the substrate instead of using glue.

To confirm and quantify the performance increase using this new design, Kjeang et al. [34] wrote another paper shortly after where the exact same flow field design and prototype were used but using different types of electrodes to compare them: flow over graphite electrodes and porous flow through electrodes. The exact same fabrication method was used as well for both of them. Flow over graphite electrodes performance was compared against the flow through porous electrodes using the same testing conditions and apparatus. The flow over performance and fuel utilization were significantly below the flow through electrode design.

This promising architecture however raises some concerns: having a parallel flow design for the waste channel in between the electrodes allows diffusion, that might happen in the central waste channel and create fuel cross over which decreases the performance as unwanted reactions happen at each electrode (cathodic reaction happening at the anode electrode and vice versa). The distance between the two electrodes (1mm) is also significantly contributing to ohmic losses as the ionic ohmic resistance increases with the distance between the anode and the cathode electrodes. Salloum et al. [15] responds to these issues by introducing a counter flow design which includes a third fluidic input, where highly conductive, but non reactive electrolyte is injected in the proton exchange area of the channel (higher concentration of H_2SO_4). This architecture is opposite to the parallel architecture where ohmic losses are high, by minimizing the distance between the catholyte and anolyte mixed with a highly ionic conductive electrolyte. The electrolyte input also prevents fuel crossover at the same time by having a third stream source that

mixes with the fuel and oxidant streams. However, the third input is adding complexity to the system in terms of micro piping and waste management. This system is also more sensitive to flow rate impact on fuel utilization due to a smaller electrode length. The comparison in terms of performance is not consistent with other papers as the fuel concentration used was significantly lower in this case (50mM vs 2M in the Kjeang et al papers). This design is also using flow through electrodes, as it is the design that allows the highest surface contact area suited for vanadium micro fuel cell applications so far. Unfortunately, this design prevents any fuel and oxidant recycling possibilities, as it has a third input that dilutes the species in the electrolyte solution over time.

1.2.5 Vanadium microfluidic fuel cell scale up

Scale up of vanadium microfluidic fuel cell was first investigated by Kjeang et al. [33] using a flow over design and multiple graphite rods where cross sectional view can be seen in Figure 5.

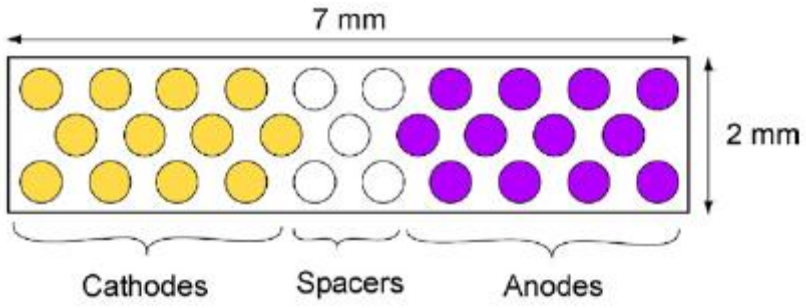

Figure 5: Cross section of the fuel cell rod array [33]. Copyright Elsevier (2007).

Compared to flow over unit cell, this is a major improvement in terms of performance and fuel utilization. However, this work was completed prior to the flow through [35] design, where the active area is maximized, increasing the reaction surface as well as reducing the mass transport losses, which highly improves the performance and fuel utilization.

Flow through based design scale up was investigated by Salloum et al. [16] in 2011 where individual fuel cells were fluidically connected in series as illustrated in Figure 6.

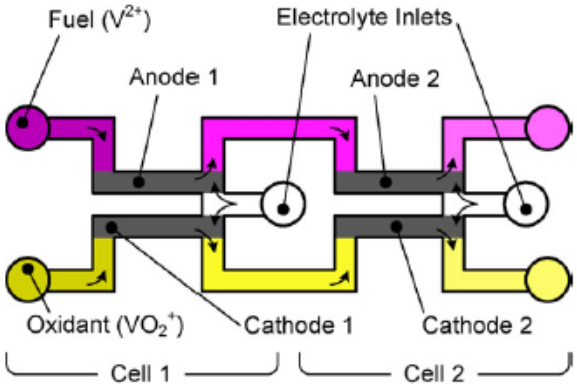

Figure 6: Microfluidic fuel cell array [16]. Copyright Elsevier (2011).

The fuel utilization of the single-cell counter flow architecture Salloum et al. first developed in 2010 was limited to 12%, a two-cell array cell configuration addresses this issue by passing the unused fuel and oxidant from the first cell to a second cell connected fluidically in series, thereby effectively doubling the fuel utilization [16]. The performance of the second cell was lower than the first cell as the fuel and oxidant were less concentrated; however, the overall fuel efficiency of the system was increased. Because of the performance difference, the cells were connected in parallel, running at constant voltage with different current produced from each cell. The current and power output of the device was thus nearly twice as high while the voltage was the same as for a single cell. A disadvantage of this configuration is that an additional pressure-driven blank electrolyte stream is required for each consecutive cell in the array.

Another flow through scale up solution has been investigated by Moore et al. [36]. In this study using a flow through design, the individual cells are fluidically and electrically connected in parallel. The design adopted is a dimensional scale up to an active area of 1cm² using stacked carbon fibre paper as electrodes to achieve different thicknesses, which was then compared with carbonized Kapton (Dupont) by pyrolysis used as electrodes.

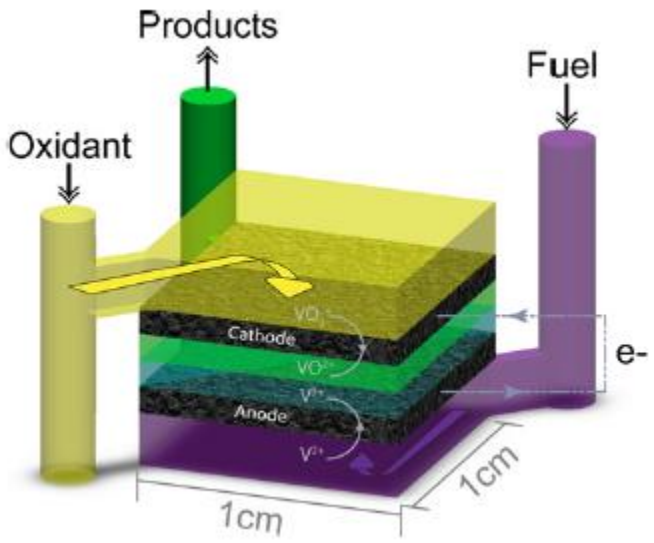

Figure 7: Unit cell design [36]. Copyright Elsevier (2011).

In Figure 7, we can observe the design of a unit cell used in this study. This design took into consideration cost reduction with symmetric manifolds, reducing the parts diversity, and keeping in mind scale up options such as stackable unit cells similar to PEM conventional hydrogen fuel cells. This newly designed unit cell achieved performance of 15.7 mA/cm² and 5.5 mW/cm² at peak current and power densities. It was also built twice and connected in parallel, with independent flow systems for each cell. Almost double the performance was obtained. Some losses (up to 30%) were attributed to a non balanced fuel distribution between both cells and differences due to manufacturing in the electrode thickness and uniformity.

1.3 Objectives

This thesis presents microfluidic vanadium fuel cell scale up solutions. The goal is to develop scale up solutions for the flow through membraneless microfluidic fuel cell technology developed by Kjeang et al. [35] while trying to match the same performance. With very promising results such as a power density value achieving up to 131mW/cm² and low manufacturing cost, this technology would fit perfectly for commercial application, notably for portable electronic applications.

Scaling up is a major step and challenge needed for this technology, in order to bring it closer to commercialization. With many different fuels and oxidants used and successfully demonstrated using this technology, we decided to use vanadium based reactants for both oxidant and fuel as its regenerative capabilities within the same cell makes it more attractive for numerous reasons and for different applications. The device could run as a fuel cell as well as a flow redox battery. By running the flow backwards and applying the proper voltage, the device can run as an electrolyser and charge the electrolyte back to its initial state. The electrochemical kinetics of vanadium redox reactions are also high enough to eliminate any need of catalyst, which simplifies the system while significantly decreasing costs.

This dissertation presents two major scale up approaches:

-Multiplexing (using 2 cells) that fluidically connects all the cells composing the array in parallel, using a fluidic analysis to overcome the flow distribution uniformity challenge for each cell, that is crucial to achieve a steady and balanced performance, as well as manufacturing processes that are high volume compatible such as laser etching and microfabrication methods that include photolithography.

-Dimensional scale up that increases the active area volume by about a hundred times. This approach is very challenging and has not been successfully addressed yet because of the difficulty to keep a microfluidic co-laminar flow at larger dimensions, and spread the liquid reactants evenly on such a large surface.

The scope of this work does not include any improvements to the design of the unit cell [35], and tries on the contrary to keep the unit cell design untouched when our equipment and materials available permits it for the multiplexing approach.

2. SCALE UP SOLUTIONS

Two complementary approaches are investigated for scale up solutions: a multiplexing approach, and a dimensional scale up approach. In both solutions, the reactants flow distribution uniformity is the main challenge, in order to stabilize the performance and allow a steady state operation.

2.1 Multiplexing approach

Contrary to electrical engineering field, multiplexing in our case just refers to linking and adding unit cells together in any direction to form an array of cells.

In the multiplexing approach, Salloum et al. [16] connected two cells electrically in parallel and fluidically in series. The multiplexing solution we chose to adopt is not based on cells linked fluidically in series as this option is decreasing the reactant concentrations after passing through each cell. The performance of each cell composing the array is hence not equal. This can create issues when trying to integrate these energy sources in a unified system, as explained earlier. An unbalanced array is dragging the performance down.

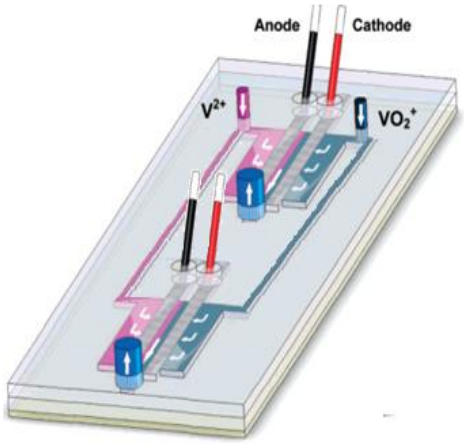

Figure 8: Fuel cell array multiplexing solution

In our design, greatly inspired from Kjeang et al. design [33] illustrated in Figure 8, we try to obtain a balanced array, where each cell composing the array is receiving an equal concentration of reactants, at an equal flow rate. In that case, each cell composing the array is sharing the inlet flow equally. When fluidically connecting them in parallel with an equal flow rate sharing (50%-50%), each cell of the planar array has the same theoretical performance, which facilitates the electrical system integration by simply connecting each cell in series. In this case, the array is balanced. All the individual cells are running at equal performance, so no weak cell is dragging the whole array performance down.

In the multiplexing approach, in order to reach the flow uniformity for each cell of the array, the solution that was adopted is to have a fixed flow rate and fixed electrode dimensions, while changing the channel design. We could also use check valves placed at the outlet of each cell in order to control the back pressure of each cell and achieve a uniform flow distribution. Multiplexing could have been done using natural symmetry axis such as the back to back design shown in Figure 9, however, this option limits the multiplexing. Adopting a non symmetrical multiplexing option allows us to expand further with a greater number of cells than the symmetrical multiplexing.

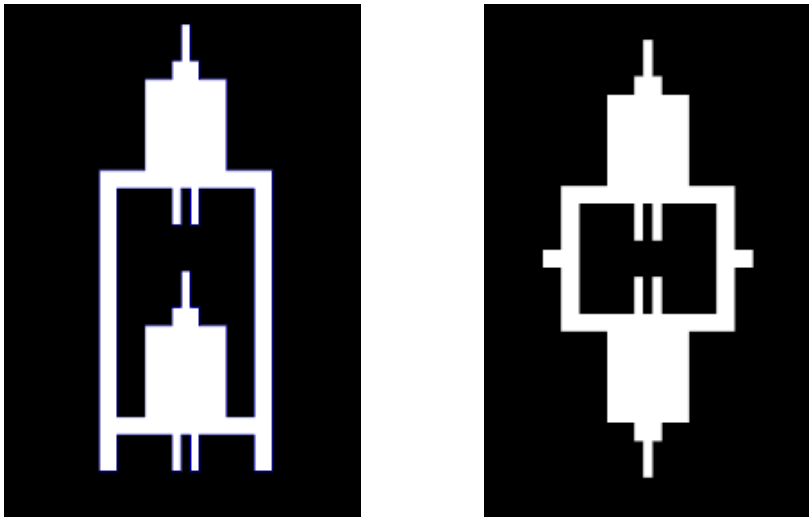

Figure 9: Non symmetrical multiplexing (left) vs. symmetrical multiplexing (right)

The electrodes (Toray TGP060) used are 1 mm wide and 1.2 cm long. The array thickness (channels and electrodes) is 140 μm thick, which slightly compresses the

electrode to minimize reactants to flow over and under the electrodes and forcing the flow through the electrode instead, as desired.

Non heat treated electrodes were first tested, while heat treated electrodes (passed under a flame) were finally adopted as they are more hydrophilic, which resulted in a slight performance increase.

2.2 The dimensional scale up approach

The dimensional scale up is based on increasing the size of the unit fuel cell, which seems a more natural way to scale up. The fibrous carbon paper electrodes orientation was flipped by 90 degrees in order to increase the cross sectional active area. The reactants are then flowing across the electrodes in the through plane direction as described in Figure 10 whereas they were flowing across the electrodes in the in-plane direction in the multiplexing approach.

The challenge in this approach is to keep the microfluidic co-laminar regime and properties effective at a much larger scale where gravity has a greater impact, while distributing the reactants evenly on the larger surface at the same time. To fulfill those conditions, some materials and designs were investigated. The final design consists of a first wicking hydrophilic layer that distributes the reactants evenly on a larger planar surface, while having a high permeability to facilitate the flow. This layer is crucial as the dimensional scale up is significant enough to have channels where microfluidics reaches its limitations: the impact of the gravity cannot be neglected anymore as it becomes predominant compared to surface tension forces.

Then, the electrode thickness is increased, using a layer that has a higher pressure drop (or lower permeability). Several materials were investigated: porous carbon plates and layered TGP 060 (both heat treated and untreated).

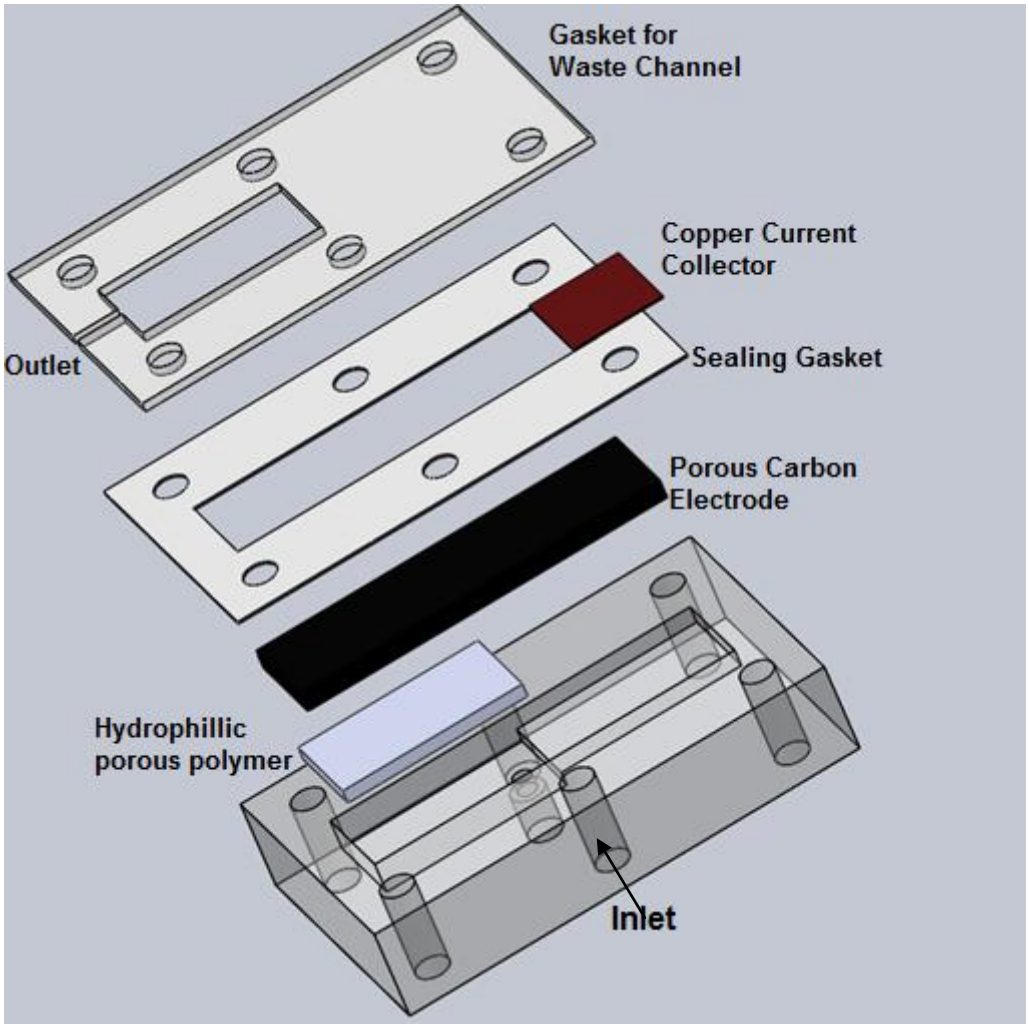

Figure 10: Dimensional scale up solution (half of the cell shown).

The wicking layer is 1.8 mm thick, the surface of the active area is 2 cm² (2 cm long, 1 cm wide, and 1.8 mm thick). The actual length of the electrode is 4 cm. Half of it serves to transmit the current to a copper current collector, shown in red in Figure 10. The waste channel where reactants in a co-laminar flow regime exchange protons is 1 mm wide.

3. FABRICATION METHODS

Another aspect of this work is to use fabrication methods compatible with the industry standards and well demonstrated techniques for high volume manufacturing. Microfabrication techniques such as lithography, and laser cutting were the manufacturing methods considered and tested in order to build our planar array (multiplexing scale up). An automated 3D printing machine was used to build the dimensional scale up prototype substrate.

3.1 Laser cut PMMA

The laser cutter in the small machine shop (room 4272 in Surrey campus) was used to build the very first prototypes, when the photolithography equipment was not yet available.

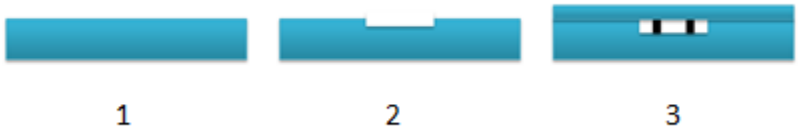

Figure 11: Laser cut PMMA fabrication process

Laser cutting (Versa Laser from Universal Laser Systems) was used on PMMA (transparent hard plastic) substrate (1) to draw the channels design inside it (2), and then bonded using hot plates (Torrey Pines Scientific) under pressure (3). This method was first used and several prototypes were successfully tested. Settings were set to 70% power for the laser, with fast sweeping to avoid burning the substrate. Several passes were needed in order to achieve the desired channel depth. We chose this fabrication method as it is compatible with high volume manufacturing. The results are not that reliable and accurate with our current equipment, as the repeatability was very low using the exact

same settings, but this method should still be considered with a better laser cutter for future development.

The performance was promising, but not comparable to previous literature results, as the laser cutter we had available in our lab was not providing us with a smooth surface at its highest resolution. The surface of the channels using this fabrication method with our onsite laser cutter was very rough. Flow over and under the electrodes was strongly suspected to happen, decreasing the electrode utilization, overall efficiency and performance.

Holes for inlet and outlet fluids and electrical wires are drilled just after step 2. Electrical wires are glued to the electrodes and substrate using silver (conductive) epoxy.

3.2 PDMS molding

PDMS is a soft plastic available commercially in liquid form. After pouring it on a master mould, we can get the shape we need after it is cured.

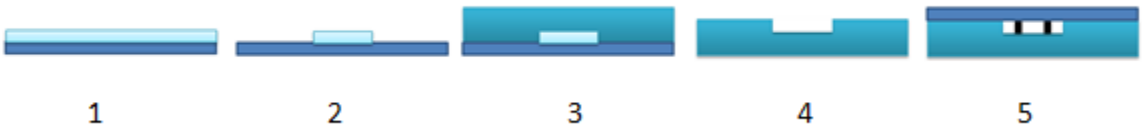

Figure 12: PDMS molding fabrication process

The master was first built with SU-8 2100 photoresist (Microchem) coated on a glass substrate (1), using a spin coater (G3P-8, Specialty Coating Systems Inc.). In order to keep the best consistency and avoid bubbles, 8 ml of SU-8 that was previously degassed in a 30 ml syringe overnight, was used for each master. The settings used to achieve the best thickness uniformity were 300 rpm/sec ramp for 30 seconds, 1700 rpm dwelling time for 30 seconds, and 25.5 seconds for the deceleration time to reach complete stop. After a pre-bake at 55°C for 4 hours and 60°C for another 4 hours to avoid excessive solvent evaporation that creates big puddles, the substrate with a uniform SU-8 coating is placed

under a UV exposure unit (LS 150-3 NUV, Bachur and Associates) with a mask, for a duration of 10 seconds at 350 W. After the post bake (55°C for 30 minutes and 60°C for another 30 minutes), the master is developed using a SU-8 developer (Microchem) and cleaned (2). With the master ready, PDMS (Sylgard 184, Dow Corning) is poured on the master, degassed and cured for 48 hours in a vacuum oven at ambient temperature (4). After carefully peeling the PDMS substrate off the master and placing the electrodes, plasma treatment using a corona discharger (Model BD20, Electro Technic Products Inc.) is applied on the surface of the PDMS surface for 2 minutes. A clean glass substrate is then applied on it under pressure for 24 hours (5).
Similarly, the holes for the fluidics (inlet and outlets) and the wiring are poked through the PDMS just after step 4, using a die cut, and electrical wires are glued to the electrodes with silver epoxy (MG Chemicals). PDMS was moulded on the master to obtain a smoother surface prototype compared to the laser cut PMMA, in order to avoid flow over and under the porous electrodes, enhancing the flow through which results in a better use of the entire 3-D volume.

The challenge in this method is trying to achieve a uniform thickness over the whole area, with the equipment available in our lab. An extensive trial and error method was used in order to identify and determine the final parameters to achieve a uniform thickness. The thickness was measured with both a micrometer (Mitutoyo) for quick measurements and double checked on a profilometer (SJ-400, Mitutoyo) that provide higher quality and resolution measurements. The results using both devices were however comparable (within 5 μm difference).

However, perfect thickness uniformity is hard to achieve, and height differences that generally are up to 15 μm were observed.

3.3 PMMA Patterning

UV impregnation of patterned PMMA using microfabrication techniques which allowed us to obtain a very smooth surface more easily was proposed by Marius Haidicu, a PhD

student in Engineering Science at SFU Burnaby, who greatly helped us to develop this fabrication method [37,38].

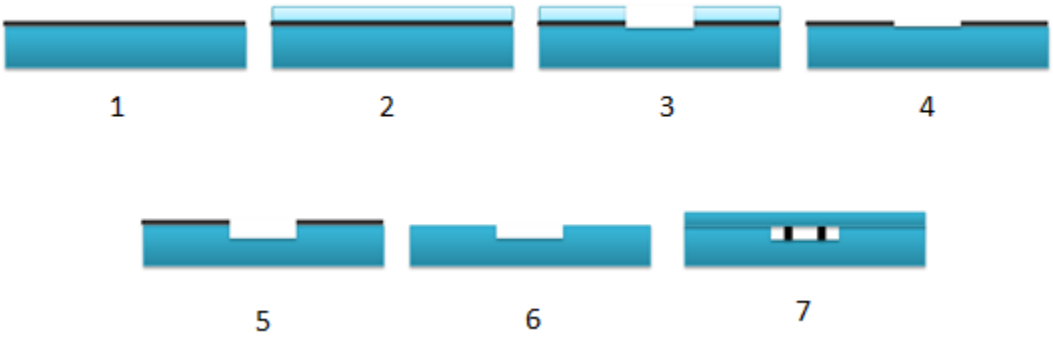

Figure 13: UV exposed PMMA fabrication process

For this work, 3" X 3" pieces of mirrored PMMA were used. This substrate was acquired from Paskolite Inc., the brand name of it being Optix®. This mirrored acrylic comes with a 120-150 nm of aluminum already coated on it (1). After an initial cleaning step consisting in substrate immersion in a methanol bath for 10-15 minutes, the metal film is patterned using classical photo-lithographical techniques. This patterning creates a metal hard mask, which is later on used to irradiate selectively the acrylic substrate underneath the metal film with deep-UV.

The metal patterning starts with spinning on it positive photoresist (Shipley 1813) followed by a 5 min. pre-bake step at 100 °C (2). The substrate is then exposed to near UV (365 nm) for 30 seconds through a mask that features the desired patterning layout. After this exposure, the irradiated photoresist is washed away in a developer bath and the substrate is transferred into a bath containing aluminum etchant (3). In case a standard cleanroom aluminum etchant is used, this step does not take more than 2 minutes, given the thickness of the aluminum film. To clean up the remaining photoresist on the surface of the substrate, a flood near UV exposure followed by a development step is applied (4). Now, the substrate is ready for deep-UV irradiation (5).

The deep-UV exposure is performed using an in-house built irradiation box, equipped with germicidal lamps whose main component of the emitting spectra is at 253.7 nm. The length of the deep-UV irradiation step was chosen to be 48 hours, which, considering the

power of the lamps and the distance between the substrates and the lamps, gave to the substrate an irradiation dose of 1500 J/cm^2. The deep-UV irradiation inflicts backbone scissions in the polymeric chains, lowering PMMA's molecular weight. Shorter PMMA chains can be washed away in a developer bath, which consists of a mixture of isopropylic alcohol (IPA) and water at a ratio of 7:3 (5). After the desired depth of the channel is achieved, the aluminium layer that served as a hard mask is removed during an etching step (6). The channel depth is measured using a stylus profilometer.

Similarly to the laser cut PMMA fabrication method, holes were drilled just after step 6, to allow for fluidic and electrical wires to reach the electrodes. Electrodes were aligned and another PMMA part was bonded to seal everything. Bonding involved either compression on a hot plate, microwaving or acetone bonding of the PMMA plates. Microwaving and acetone were abandoned as the bonding quality suffered most of the times. The details of this fabrication process are still under development; hence, no conclusive experimental data have been obtained using this method. This method needs more improvements, but it is a potentially reliable way of manufacturing our prototypes.

3.4 Dimensional scale up - 3D printer

For the dimensional scale up approach, a 3D printer available in SFU premises was used to manufacture the substrate. The quality of the plastic used for the substrate was crucial. Low grade plastic that is too porous was allowing vanadium electrolyte to pass through which caused high amount of leaking. Several attempts were necessary in order to get a higher quality substrate.

Once the substrate is available, a layer of hydrophilic porous polymer (plasma treated by the supplier: Porex, Model x-4897 and x-4588) serves as a first buffer layer. The material in itself is lightly deformable, which improves the sealing, and the average pore size is 15µm. Its main purpose is to spread the reactants as evenly as possible over the whole active area. The electrode is the second layer. The pressure drop of this layer is higher, which allows the liquid to spread more evenly inside the first layer. The reactants can

then slowly diffuse and permeate through the porous electrode layer. Three prototypes with electrodes made of three different materials were used: a solid graphite plate, compressed layered untreated TGP 060 (Toray carbon fibre paper) and compressed layered heat treated TGP 060 (enhances its hydrophilic properties). As the material used for the electrodes needs to be acid resistant while conducting electrons, carbon based materials well known in the fuel cell industry were chosen.

The graphite plate (Selee Corporation) has a porosity of 30%, a permeability of 2×10^{-19} m^2 and an average pore diameter of 1.5 microns (manufacturer's data). The carbon fiber paper (from Toray) has a porosity of 78% and a permeability of 1.28×10^{-11} m^2 [39]. This material is the same as the electrodes used in the multiplexing approach. The current collectors used were made of copper, and the waste channel has a width of 1 mm. The active area size is 2 cm^2; and the electrode thickness is 1.8 mm. Sealing was ensured by three silicon gaskets, that also allow a gap of 1 mm for the waste channel. The whole device was held under compression using 6 bolts and nuts, with higher compression on the current collector side to prevent liquid reactants from going upstream and corroding the current collectors.

4. FLUIDIC ANALYSIS

The real challenge of the multiplexing scale up solution is to obtain a uniform flow distribution for all the cells composing the planar array, while keeping a co-laminar, microfluidic flow regime. Fully developed laminar pipe flow theory was used to calculate the pressure drop across the channels, as the aspect ratio is high enough. Darcy's law was used to calculate the pressure drop across the porous electrode. A computational fluid dynamics software (Fluent) was used to predict the flow analysis. Those results were compared to the theoretical results, as well as verified with experimental work using vanadium electrolyte in the prototype.

4.1 Theoretical analysis

4.1.1 Channel pressure drop analysis

When multiplexing the cells and fluidically linking each unit cell in parallel, each cell is fed with reactant of a given concentration, but at different rates due to the losses induced by the friction of the fluid on the channels walls. In order to achieve a uniform flow rate (and hence, a uniform pressure distribution) for each cell, the channel design has to be modified. To facilitate this study, we convert the problem as an electrical circuit, where the voltage would be the pressure drop (dP), the current would be the flow rate (Q), and the resistance would be the resistance seen by the flow (R) on each section of the channel. Then Ohm's law would be adapted: U=RI becomes dP=RQ. Each section of the channel is converted into a resistor (Figure 14). Because of the device's inherent symmetry, the study is made on half of it to save some analysis and modeling processing time. The device will be composed of a mirror image of itself along the bottom horizontal axis.

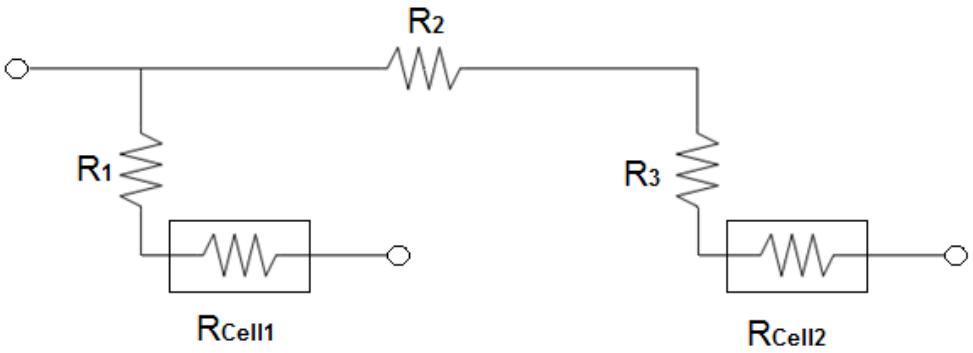

Figure 14: Microfluidic fuel cell electrical equivalent circuit (half of the array)

To achieve a uniform distribution, provided that both cells that composes the array are identical (Rcell1=Rcell2), we must fulfill R1=R2+R3, where R1, R2 and R3 are the fluidic resistance of the channels.

The following two equations use the relevant internal laminar flow theory to calculate the flow resistance in the inlet channels, assuming that the flow is steady, incompressible, and fully developed. Low Reynolds numbers in the order of ~ 0.01 - 1 are expected for the characteristic flow rates of microfluidic fuel cell devices. Because of the predominantly rectangular shape of microfluidic channels, the hydraulic effective diameter is used in the resistance calculations as seen in Equation 1, and the hydraulic diameter Dh is given in Equation 2:

$$\frac{\mathbf{dP}}{\mathbf{Q}} = \mathbf{R} = \frac{\mathbf{k\,\mu L}}{\mathbf{2AD_h^2}} \tag{1}$$

$$\mathbf{D_h} = \frac{\mathbf{4A}}{\mathbf{P}} = \frac{\mathbf{2ab}}{\mathbf{a+b}} \tag{2}$$

Here, μ is the fluid viscosity, L is the length of the channel, k is 82.34 for a rectangular channel with the present width/height aspect ratio [40], A is the cross-sectional area, and P the perimeter of the channel cross-section with sides a and b. As the channel aspect ratio is high (2 mm wide and 140 μm high, equal to a ratio of 14), the option of simplifying this problem as flow between two parallel plates is also considered, calculated, and compared, using k = 96 [40].

The ratio for these values can then be optimized in order to achieve a uniform flow distribution, and a new channel design with thinner inlet channel for the first cell and a wider channel for the second one was designed.

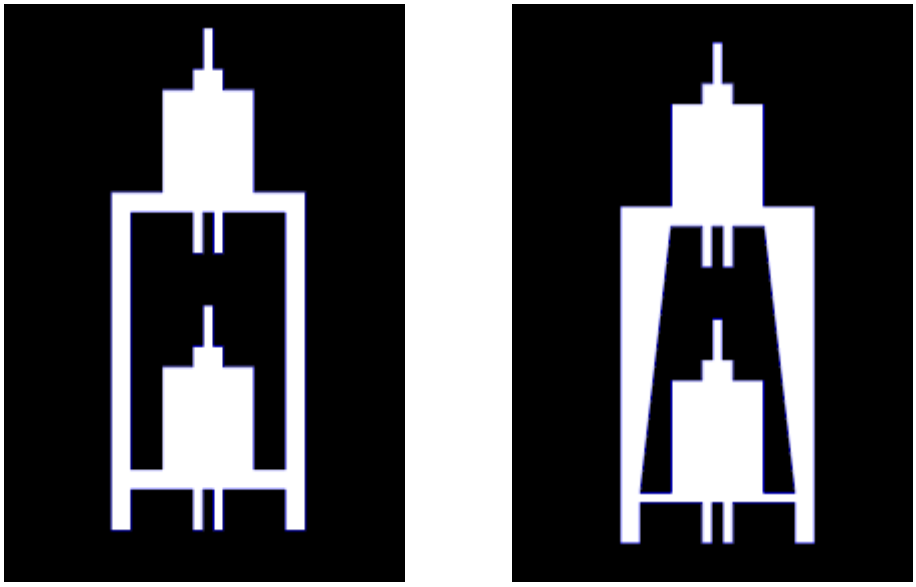

Figure 15: Masks of channel designs (left: Baseline, right: Improved design)

As seen from Equations 1 and 2, the flow resistance in the feed channel depends entirely on channel geometry and is independent of flow rate and mean velocity. More specifically, the flow resistance is a function of the length and the width of the channel, provided that the channel height is generally fixed in microfabrication and ought to be considered a constant determined by the optimum unit cell design, in the present case 140 μm. The ratio for these values can therefore be optimized to achieve matching flow resistances for each cell and hence a uniform flow distribution for the array. In the improved prototype, the bottom cell inlet channel is only 1 mm wide for a 4 mm wide channel for the top cell (Figure 15). By increasing the flow resistance of the bottom cell while decreasing it for the top cell, we managed to obtain a design close to a uniform pressure distribution for both cells. Many combinations are possible in terms of channel design, but in order to keep the changes as minimal as possible from the baseline design, the dimensions presented above were the best fit.

4.1.2 Porous electrode pressure drop analysis

Darcy's law was used in order to calculate the pressure drop across the carbon porous electrodes.

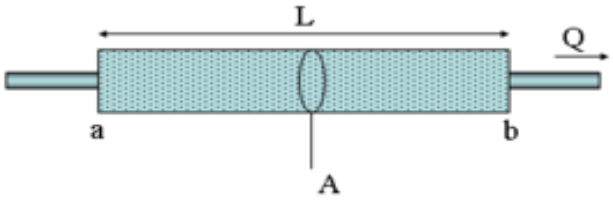

$$\frac{\mathbf{dP}}{\mathbf{Q}} = \mathbf{R} = \frac{-\mu \mathbf{L}}{\mathbf{KA}} \qquad (3)$$

Where K is the permeability, L is the length travelled by the flow inside the porous media and dP = Pb-Pa is the pressure drop.

In our design, the active part of the electrode is 1.2 cm wide, and 1 mm long. The channels are 140 μm high. Viscosity of vanadium was taken to be 0.008 kg/m/s [41], and the permeability of the carbon electrode (TGP 060 untreated) taken is 1.28e-11 m² [39].

4.2 Computational Fluid Dynamics (CFD) Analysis

After having a first attempt at building a fuel cell array by simply connecting 2 unit cells in series, we clearly saw that the flow distribution was not balanced at all, as expected. CFD modeling was needed in order to address that issue.

We use a 3D laminar flow model in our analysis. Incompressible steady state laminar flow was assumed, with mass and momentum conservation as follows:

$$\nabla \cdot (\rho \mathbf{u}) = 0 \qquad (4)$$

$$\rho \mathbf{u} \cdot \nabla \mathbf{u} = -\nabla p + \mu \nabla^2 \mathbf{u} \qquad (5)$$

Where u is the fluid velocity. As the flow is continuous, no slip conditions apply on the walls (u=0 at wall).

We chose to use FLUENT as CFD software for our work as it is based on finite volume elements. It would hence be more accurate than COMSOL that uses finite elements method based procedures to solve the case, where results are more sensitive to mesh size.

Figure 17: Fluent baseline model results

Only half of the device was modeled in order to save processing time, as it is a symmetric device (Figure 17).

FLUENT is using Ergun's equation when solving a porous media problem, assuming that it is a granular media.

$$Total\ Pressure\ Drop = Viscous\ Loss + Inertial\ Loss$$

$$\frac{dP}{L} = \frac{150\ \mu\ (1-\varepsilon)^2}{D_p^2\ \varepsilon^3}\ V\ +\ \frac{1.75\ \rho\ (1-\varepsilon)}{D_p\ \varepsilon^3}\ V^2 \qquad (6)$$

Where dP is the pressure drop across a granular based porous media of length L, μ is the viscosity, ε the porosity of the medium, Dp the average particle diameter, V the average velocity and ρ the density.

This equation can be rewritten as a simplified expression of momentum in a sink used by FLUENT:

$$\frac{dP}{L} = R_{viscous}\ \mu\ V\ +\ 0.5\ R_{inertial}\ \rho\ V^2 \qquad (7)$$

As we have laminar flow (low velocity), the V^2 term will be negligible compared to the V term. It is a fair assumption to set the inertial resistance value to 0.

As we do not want to use a granular porous media setup, R viscous can be replaced by 1/K in order to obtain Darcy's law with Q=VA. The final expression considered by Fluent is then equivalent to Darcy's law:

$$\frac{dP}{L} = R_{viscous}\ \mu\ V,\ \ with\ R_{viscous} = \frac{1}{K} \qquad (8)$$

After processing the case using different flow rates, the results obtained are compared with theoretical values in Table 1. The flow rate of each unit cell is compared with respect to the total inlet flow rate, and the ratio between the two values is how we define the flow sharing.

10µl/min	CFD dP (Pa)	Flow rate (µl/min)	Flow sharing %	Theoretical dP (Pa)	Diff. (%)
Cell 1	38.40	5.9	58.98	36.56	-5.04
Cell 2	26.71	4.1	41.02	25.43	-5.04
100µl/min	CFD dP (Pa)	Flow rate (µl/min)	Flow sharing %	Theoretical dP (Pa)	Diff. (%)
Cell 1	384.1	59	58.98	365.6	-5.07
Cell 2	267.2	41	41.02	254.3	-5.08
300µl/min	CFD dP (Pa)	Flow rate (µl/min)	Flow sharing %	Theoretical dP (Pa)	Diff. (%)
Cell 1	1152	176.9	58.97	1097	-5.01
Cell 2	802	123.1	41.03	763.1	-5.06

Table 1: Theoretical vs. modeling results across the electrodes

The typical errors between the model values and the theoretical values are about 5%. Regarding the pressure drop along the channels, using the laminar flow pipe equation, the difference between modeling results and theoretical calculations are larger. However, the flow sharing difference between cell 1 and cell 2 is 44%, which is significant enough to unbalance the flow rate in each cell and reduce the overall performance of the array. The flow sharing is shown to be independent of flow rate, in agreement with the laminar flow theory. By review of Equation 1 and Equation 3, it can be seen that the flow resistance only depends on the geometry of the channel cross-section, the length of the channel, the viscosity of the liquid, and the permeability of the porous media. For symmetric bilateral array designs all parameters are constant and the flow resistance dP/Q is therefore identical for each cell in the array, implying that the flow sharing is independent of flow rate as well as fluid properties (provided it is a Newtonian fluid). For non-symmetric unilateral array designs having variable inlet channel length, however, the cross-sectional geometry of each channel dominates the relative flow resistance. While the channel height is considered fixed due to single-chip

integration, the width of the channel can effectively be tuned in order to enhance the flow distribution.

10 µl/min	Cell 1			Cell 2		
	Theory	CFD Model	Diff. (%)	Theory	CFD Model	Diff. (%)
Pressure drop in channels (Pa) Laminar Pipe Flow	24.9	26.4	6.0	59.6	53.5	10.3
Pressure drop in channels (Pa) Flow Between Parallel Plates	29.0		9.1	69.5		23.1

Table 2: Theoretical vs. modeling results along the channels

The pressure drops along the inlet channels of the baseline unilateral array are analyzed in Table 2 based on theoretical and numerical modeling results. Two theories are investigated and compared: fully developed laminar pipe flow and laminar flow between two parallel plates. The difference between theoretical and numerical results is found to be larger than for the previously compared pressure drops across the porous electrodes, in particular for flow between parallel plates. Given the high aspect ratio of the rectangular microchannels, the uncertainty of the laminar pipe flow theory which is based on the hydraulic diameter (an empirical expression) is expected to be relatively high. When considering the problem as laminar flow between two parallel plates, the discrepancy is larger implying that the aspect ratio is not sufficiently high to consider the problem as two parallel plates. The equation used for the friction factor [40] also introduces a significant level of uncertainty (±40%) that likely contributes to the difference between theoretical and numerical modeling results. Numerical CFD simulations are thus recommended for cell array design.

Modeling results (seen on figure 18 and table 3) with the improved channel design show that this design has a better flow distribution, close to a perfectly even distribution at 10 µl/min. The results were very similar at 100 and 300 µl/min.

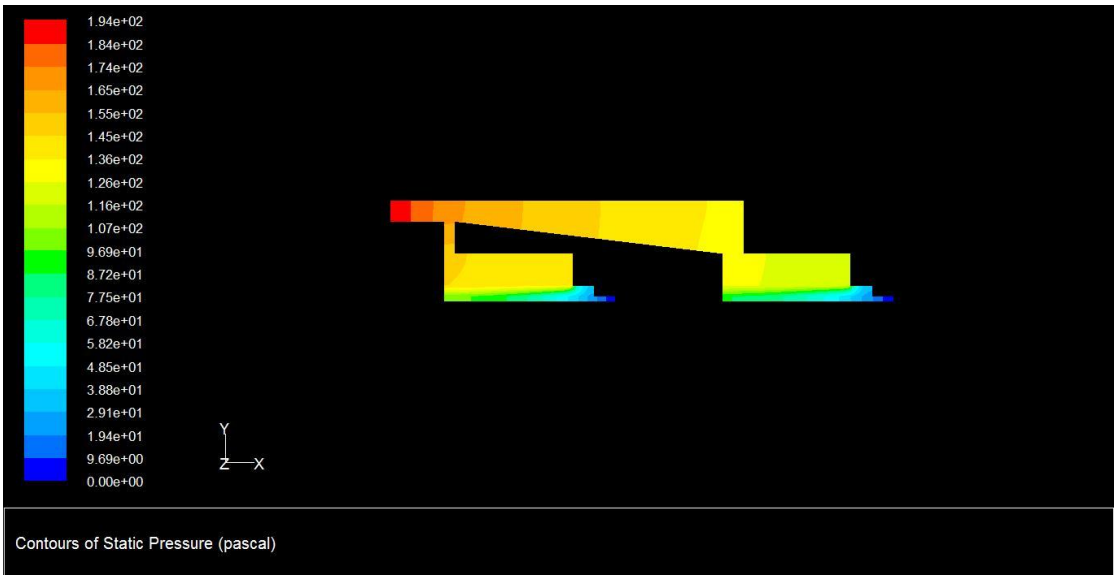

Figure 18: Fluent improved channel design results

The pressure drop across the electrodes is similar for both cells with a flow sharing close to 50%-50%.

10µl/min	CFD dP (Pa)	Flow rate (µl/min)	Flow sharing (%)
Cell 1	32.06	5.3	53.09
Cell 2	28.33	4.7	46.91

Table 3: Modeling results for flow sharing in the improved design

4.3 Flow sharing validation

To verify the modeling data, a quick fluidic experiment was conducted on a spare array prototype. An array with plugged wiring holes was fluidically tested. The outlet channels were completely removed to avoid any head pressure in the pipes to unbalance the array. The array was then flipped in order to verify that co-laminar flow was effective for both

cells. The waste obtained was collected separately and weighted in order to verify the modeling flow sharing data.

The flow sharing predicted by Fluent is 59% for the first cell and 41% for the second cell.

After testing the flow using V(V) and a V(III)/V(IV) mix having two different colors, the results were close to the ones predicted by Fluent. Respectively 64% and 36% (weight percentage). The difference can be explained by manufacturing quality and the porous carbon electrode material uniformity.

5. EXPERIMENTAL RESULTS

The fuel and oxidant used come from a commercial stock electrolyte in the V(III)/V(IV) form. The concentrations of the vanadium species are 2 M and the solution is in an acidic environment of similar concentration (4M H_2SO_4). An electrochemical charging cell is used to charge the electrolytes into V(II) and V(V) that will be used as fuel and oxidant [42]. The charging cell (or electrolyser) has a similar configuration to a conventional fuel cell with a Nafion (Dupont) membrane, and an active area of 25 cm². By keeping the voltage below 1.8 V and above 1.5 V to avoid hydrogen formation, making sure that the current was not below 20 mA to ensure a high enough conversion rate, two passes were necessary at 120 µl/min to charge the electrolyte. The electrochemical reactions are the reverse of the fuel cell operation as energy is added to the electrochemical system:

$$V^{3+} + e^- \rightarrow V^{2+}$$

$$VO^{2+} + H_2O \rightarrow VO_2^+ + 2H^+ + e^-$$

The maximum content of each species obtained are between 85 and 95% for the V(II) and between 90 and 95% for the V(V) solution. Only a limited quantity could be made at a time (20 to 30 ml a day). V(II), the lowest oxidation state of the vanadium ion is unstable in ambient atmosphere as it tends to oxidize into higher more stable oxidation states. It was always kept in a nitrogen or air seal tight environment, and used within 24 hours after it was made.

To test the multiplexing prototype, a syringe pump is used (Harvard Apparatus 11 plus) with a load bank (array of resistors). A Greenlight Innovation test station was used to test the dimensional scale up prototype.

The voltage and current density are measured and the results are plotted on a VI plot called “polarization curve”. The power against current is also plotted in order to see the maximum power the fuel cell can produce. A typical polarization curve is explained in Figure 19.

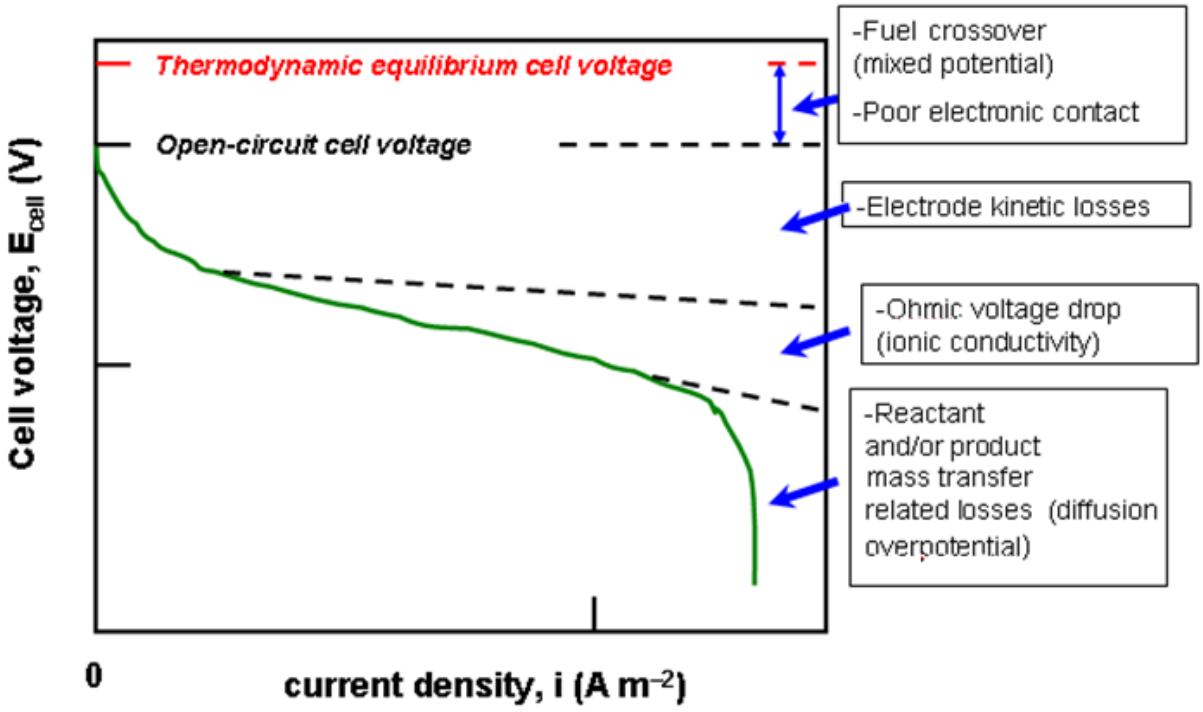

Figure 19: Sample polarization curve

Four distinctive parts can be observed on the polarization curve. A first performance drop is due to the quality of electrical contact and fuel/oxidant crossover. Then, the first inflexion point is the kinetic part (where kinetic losses occur for the electrochemical reaction to proceed), the linear part is the ohmic loss part where the resistance of components comes into play, and the last part of the curve with a bigger inflexion is the mass transport loss part, occurring as the reaction rate is being higher than the reactants supplying rate.

5.1 Multiplexing approach

Figure 20 is a picture showing the array powering a LED. When both cells of the array are connected in series, the voltage is high enough to light on the LED. The resistors on the right are used as the load bank to get the polarization curve. They are ranging from 0 to 8.2 megaohms.

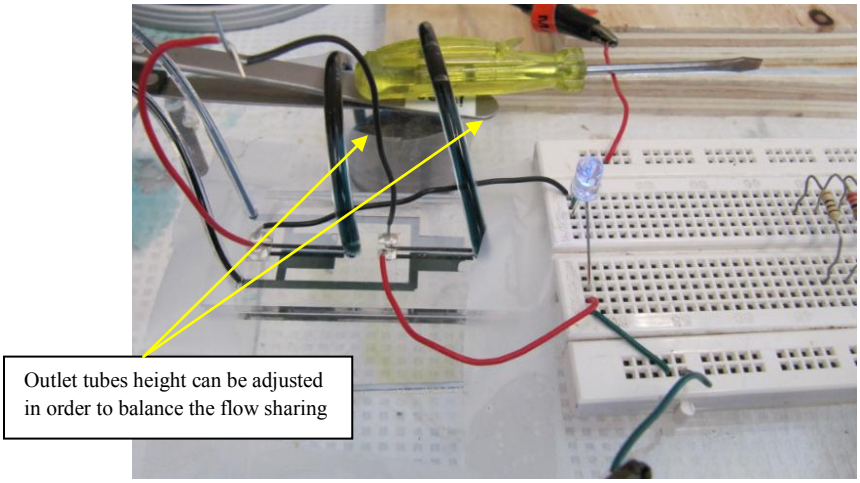

Figure 20: Image of a two-cell planar fuel cell array in operation

During the testing, each data point was taken after 1 minute to allow the fuel cell to reach steady state. Two flow rates have been tested: A low one (10 µl/min/cell), and a high one (300 µl/min/cell) in order to evaluate the performance of the fuel cell at different levels of mass transport losses. Even if the flow rate is not perfectly balanced between the cells, we can still run the array properly with all the cells having the same flow rate, by adjusting the back pressure: The waste tubes height can be adjusted to create a head pressure. Adjusting the back pressure that way allows us to perform adjustments in order to obtain a uniform flow distribution within the array for both cells by observing that the waste from each cell is exiting with the same flow rate.

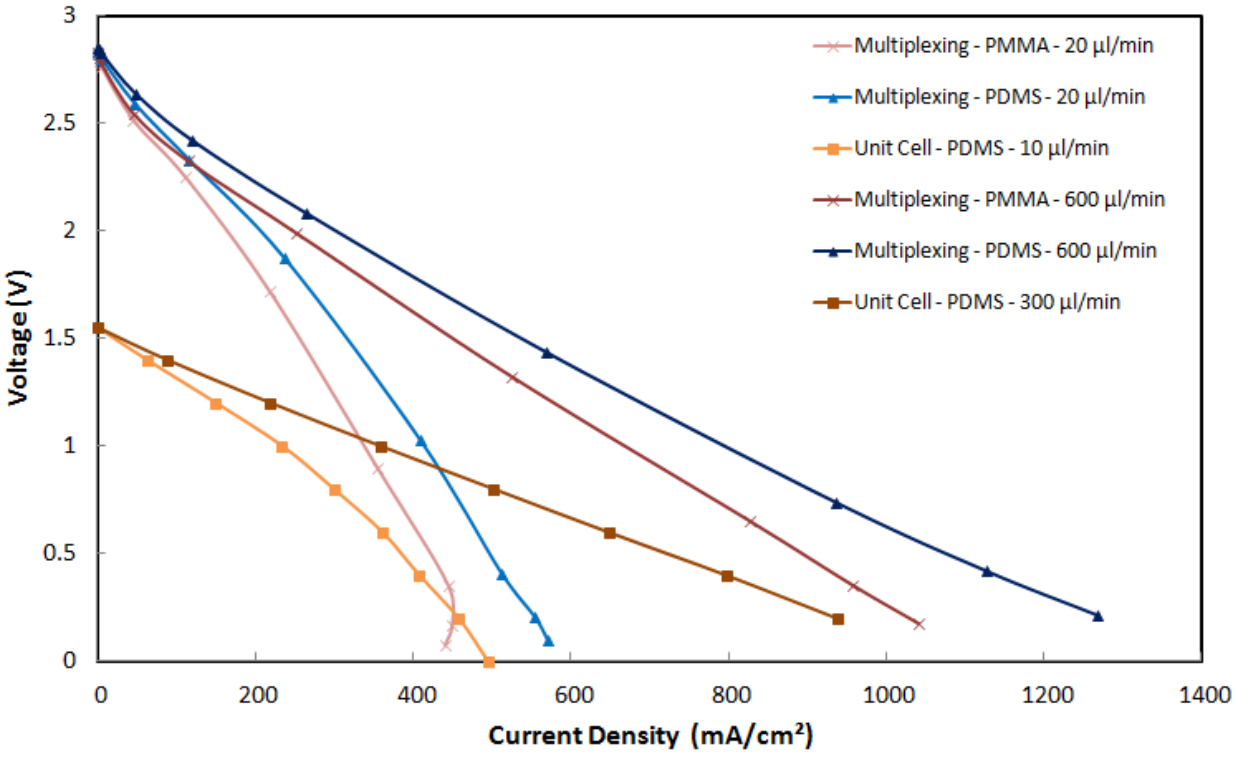

Figure 21: Multiplexing polarization curve comparison

For the prototype two-cell planar array, the flow rate was doubled in order to have a more fair comparison to the unit cell from Kjeang et al. [35], so that each cell of the array would receive the same amount of reactants as the unit cell. For comparison, the current density and power density figures were taken with respect to the cross sectional area of the electrode (140 µm high for the multiplexing array, 300 µm high for the unit cell, and 1.2 cm long for both).

As seen on the plot figure 21, a small improvement is seen between the PDMS prototype from the PMMA one, and all the polarization curves share the same trend for unit and multiplexing prototypes. The ohmic losses of the array are about twice the ohmic losses of the unit cell, as they add up to each other with the two cells connected electrically in series.

While testing multiple prototypes, it was noticed that the contact between the wires and the electrodes was crucial. If the wire is not touching the electrode, even glued together with conducting silver epoxy, the fuel cell array is not working.

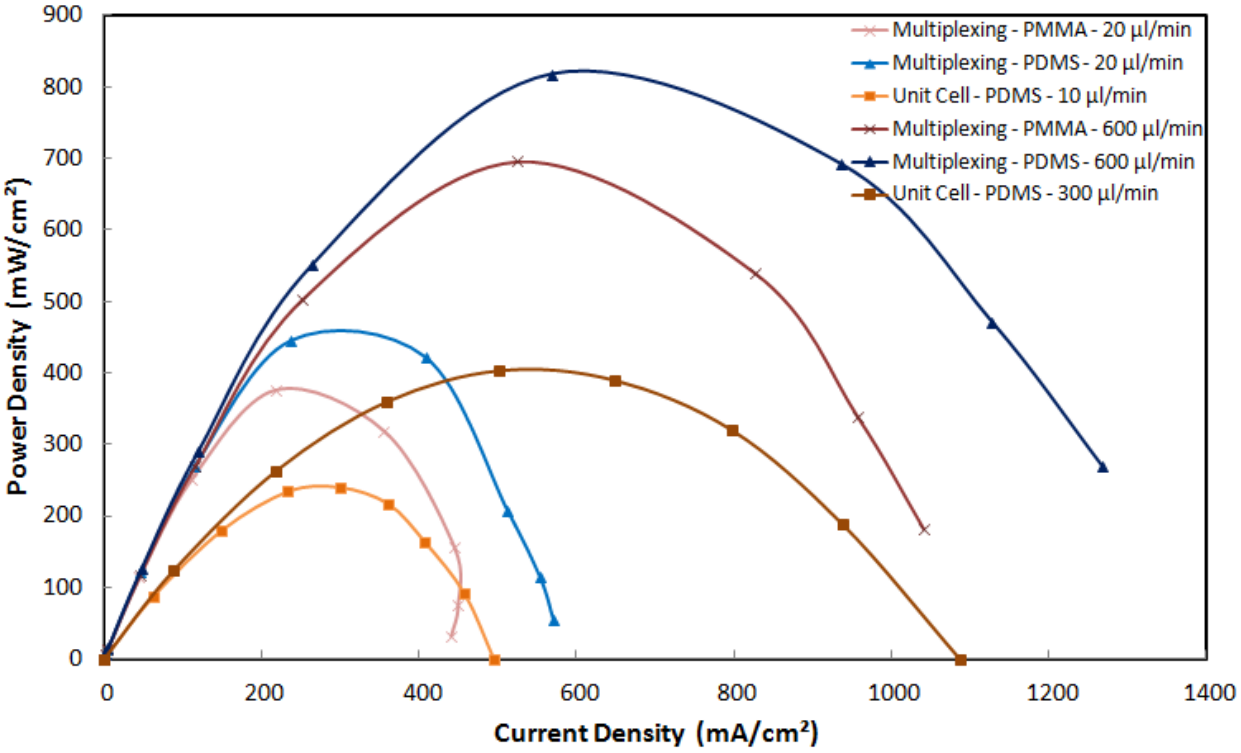

Figure 22: Multiplexing power density curves comparison

In order to compare the data from the unit cell with the data of the multiplexing and dimensional scale up option in a fair way, we have to review the way we calculate power and current density. In Kjeang et al. [35], the performance was normalized using the total projected area of the electrode (geometrical area viewed from above). In our case, we are considering the cross sectional area which is the geometrical electrode area perpendicular to the flow. Some adjustments had to be made to convert the current and power density from previously published results we need to use for comparison [35].

In the plot figure 22, we notice that the performance difference (in power density) between the PMMA array and the PDMS array is about 10% for high flow rate at peak performance which is an improvement, as the quality of the PDMS manufacturing process is higher than the PMMA one. With two cells in series in the array, the peak power density performance is close to two times higher than the unit cell. At 300 µl/min per cell, the unit cell peak power reaches 402 mW/cm², when the PDMS array reaches 817 mW/cm².

At the last data point for 10 µl/min flow rate per cell, when drawing a maximum of current, the fuel utilization for the unit cell reaches 55.4% per cell, while the PDMS array was only reaching 29.8%. When considering the thickness of the channel, the array channel thickness is lower than the unit cell channel thickness that was using TGP-090, a 300 µm thick material. The array channel height is only 140 µm as we are using TGP-060. A smaller channel means a higher velocity that decreases the fuel utilization as the residence time of the reactants in the electrodes is shorter.

5.2 Dimensional scale up

A Greenlight Innovation fuel cell test station with an external syringe pump (same as previously used for the multiplexing array with bigger syringes of 30 ml) was used in order to test the dimensional scale up cell, as the resistor load bank we used for multiplexing was not drawing enough current to get any significant power for the larger cell. One minute per data point was allowed to reach steady state for 300 µl/min, and 30 seconds for 500 µl/min. The measurement time for 500 µl/min had to be decreased as the quantity of fuel was limited.

The active area of the dimensional scale up cell represents 93 times more active volume compared to the unit cell [35], and 56 times more active area (cross section wise).

With such a large increase in scale, the main concern is to maintain a co-laminar microfluidic regime in the waste channel. To find the optimal operating point, the flow rate was gradually increased until the OCV was stable, and until any further increase of the flow rate would not affect the OCV. Several materials and configurations were tested. The very first prototype using graphite plates as electrodes was unstable. After taking the cell apart, it was noticed that the carbon porous electrodes were not permeable enough, resulting in flow over and flow under the electrodes, contrary to flow through that we were aiming for. An attempt to decrease the thickness of the electrodes by shaving the surface of it was not conclusive. As they are very fragile and brittle, many were broken when we attempted to machine them in the in-house machine shop available.

The porous carbon electrode was then replaced with multiple layers of carbon fibre paper (Toray TGP 060). A first test with these new electrodes was conclusive enough, as we managed to get a polarization curve with a flow rate of 500 µl/min. Improving the design further with heat treated porous carbon electrodes made them much more hydrophilic. The performance was improved at an even lower flow rate (300 µl/min).

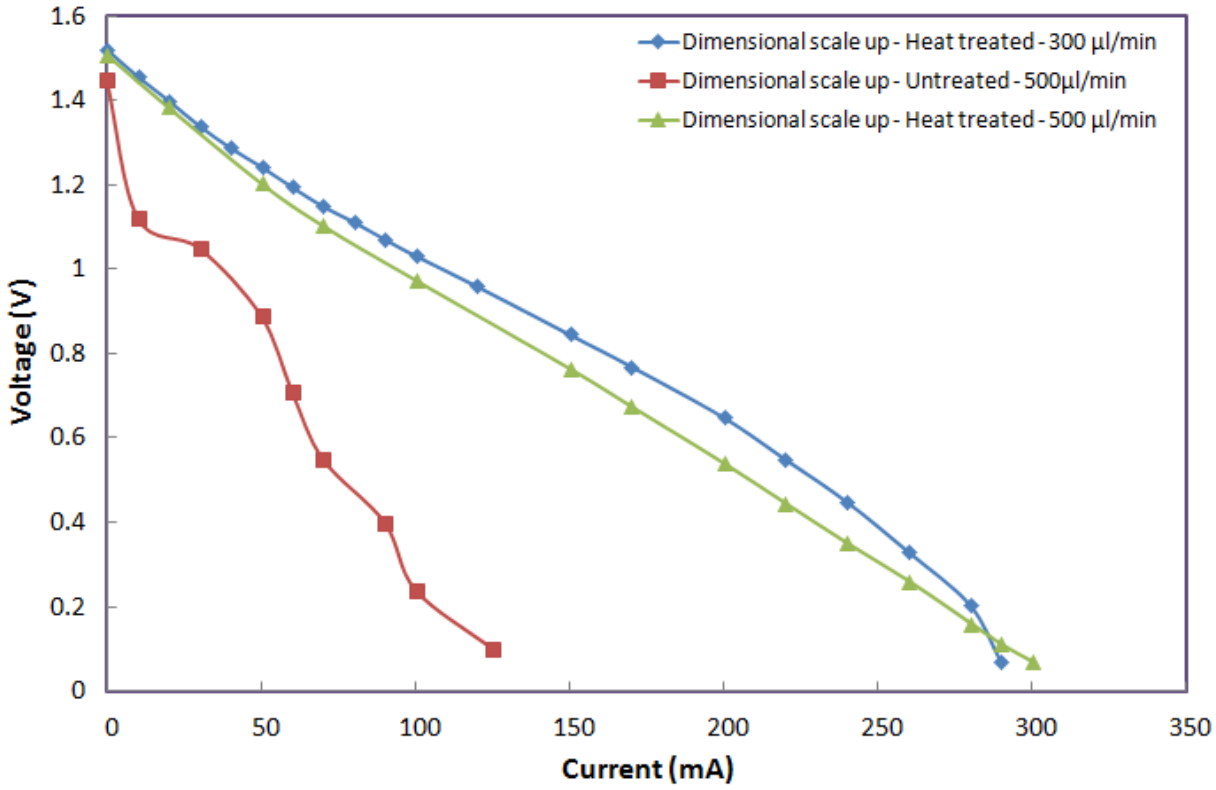

Figure 23: Dimensional scale up data

Figure 23 illustrates a clear improvement; the performance is higher with a lower flow rate, reflecting a better fuel utilization. When taking the cell apart, the cell with non heat treated electrodes was only half wet. Due to its relative hydrophobicity, only half of the active area was actually used. Whereas the cell with heat treated carbon electrodes was completely wet, meaning that the entire active area was efficiently used.

When increasing the flow rate to 500 µl/min in the heat treated carbon electrodes prototype, the overall performance surprisingly decreased. This could be explained by having disturbance in the waste channel, causing crossover losses as the co-laminar flow

could have been disturbed. The dwelling time at 500 µl/min was decreased to 30 seconds, as the fuel quantity is always limited for each test. This shorter dwelling time might be too short for the cell to reach steady state. On the hardware end, some corrosion on the copper plates used as current collector was noticed when taking apart the cell at the end of the test, and this could also have had an impact on the performance.

When comparing with the unit cell, normalizing the flow rate of 300 µl/min against the active electrode volume would be equivalent of having a flow rate of 3.2 µl/min for the unit cell.

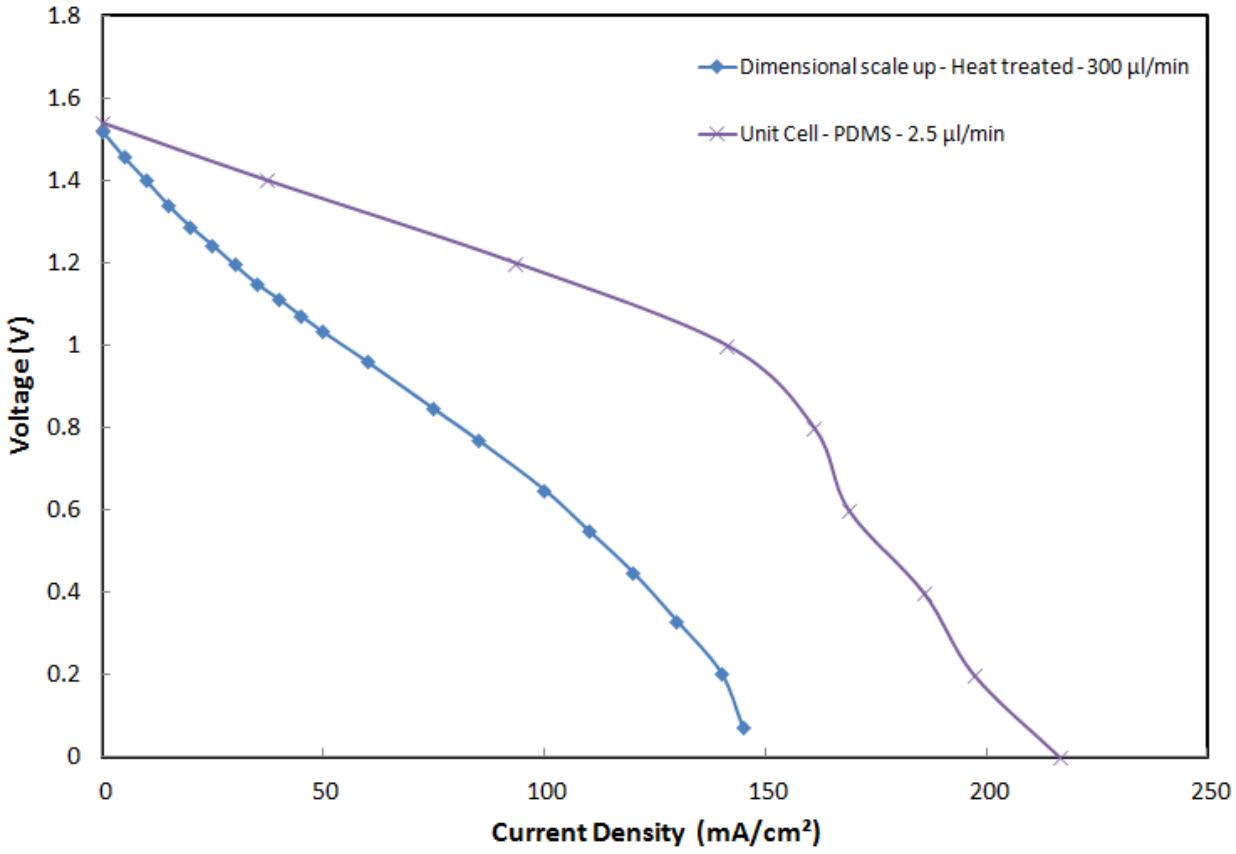

Figure 24: Dimensional scale up polarization curves comparison

Figure 24 shows that the dimensional scale up has higher ohmic losses compared with the unit cell mainly due to the much higher total current. Its larger scale and non bonded contact with the current collector can also result in discrepancies. The current collector of the dimensional scale up is compressed on the electrode, whereas it is bonded with silver

epoxy in the unit cell, enhancing the contact quality as the silver epoxy penetrates in the pores of the electrodes to some extent, increasing the contact quality between the wire and the porous electrode. In terms of size, with 4 cm long electrodes, it is more than double the length of the unit cell's electrode, and 10 times the width (1 cm vs. 1 mm) which will impact the overall resistance of the material.

Even if the dimensional scale up cell is really at another magnitude in terms of absolute performance compared with the previous results, with 93 fold volume scale up, when normalizing with respect to the cross sectional area and comparing the data, the dimensional scale up performance is still below that of the unit cell.

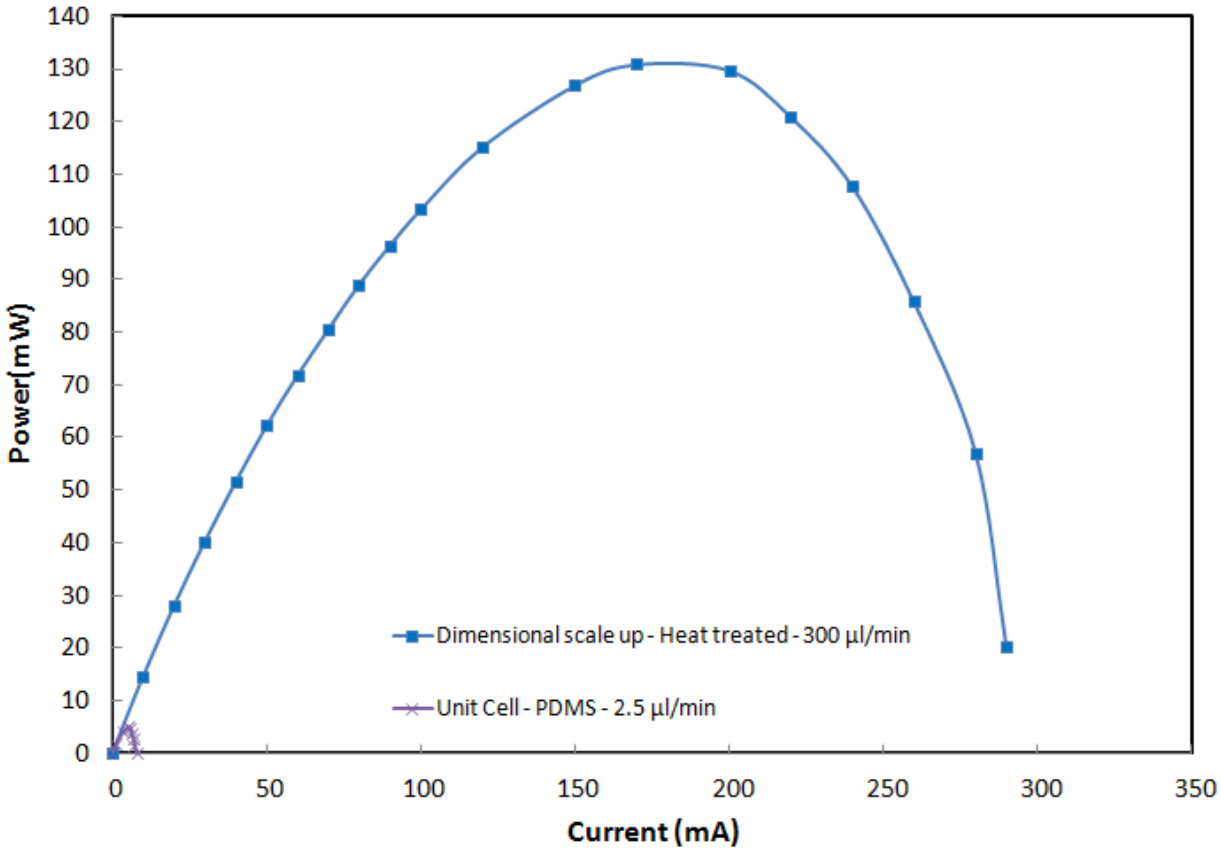

Figure 25: Dimensional scale up absolute power comparison

Plotting the performance (figure 25) shows that at peak power, the dimensional scale up reaches 130.9 mW with a flow rate of 300µl/min when the unit cell reaches 4.044 mW with a flow rate of 2.5µl/min, for a volumetric ratio of 93 times the electrode active

volume. Even if the overall power is above 100mW, which is a performance breakthrough in microfluidic fuel cells, the performance of the dimensional scale up is only 32 times higher than the unit cell for a volume that is 93 times bigger.

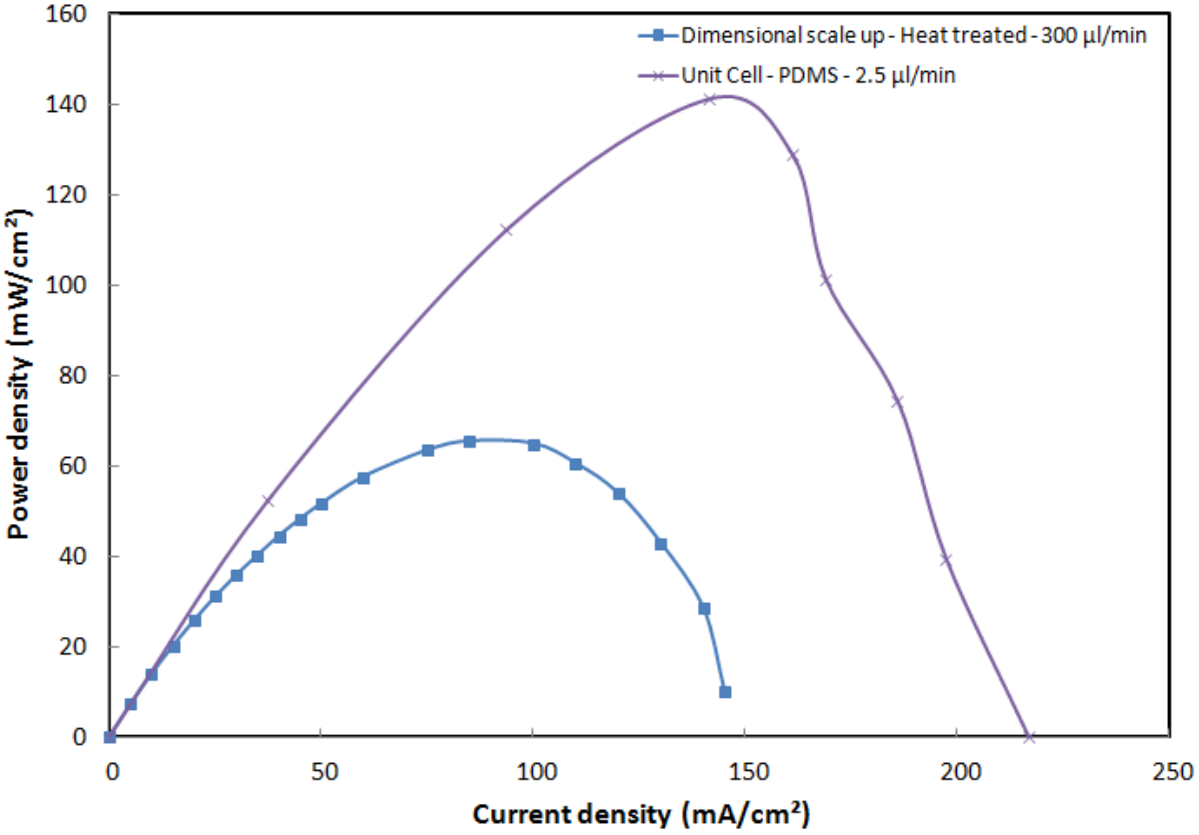

Figure 26: Dimensional scale up power density comparison

When normalizing with respect to the cross sectional area of the active region on figure 26, the trend is inverted. The power density of the unit cell is still about 2 times higher than the dimensional scale up cell.

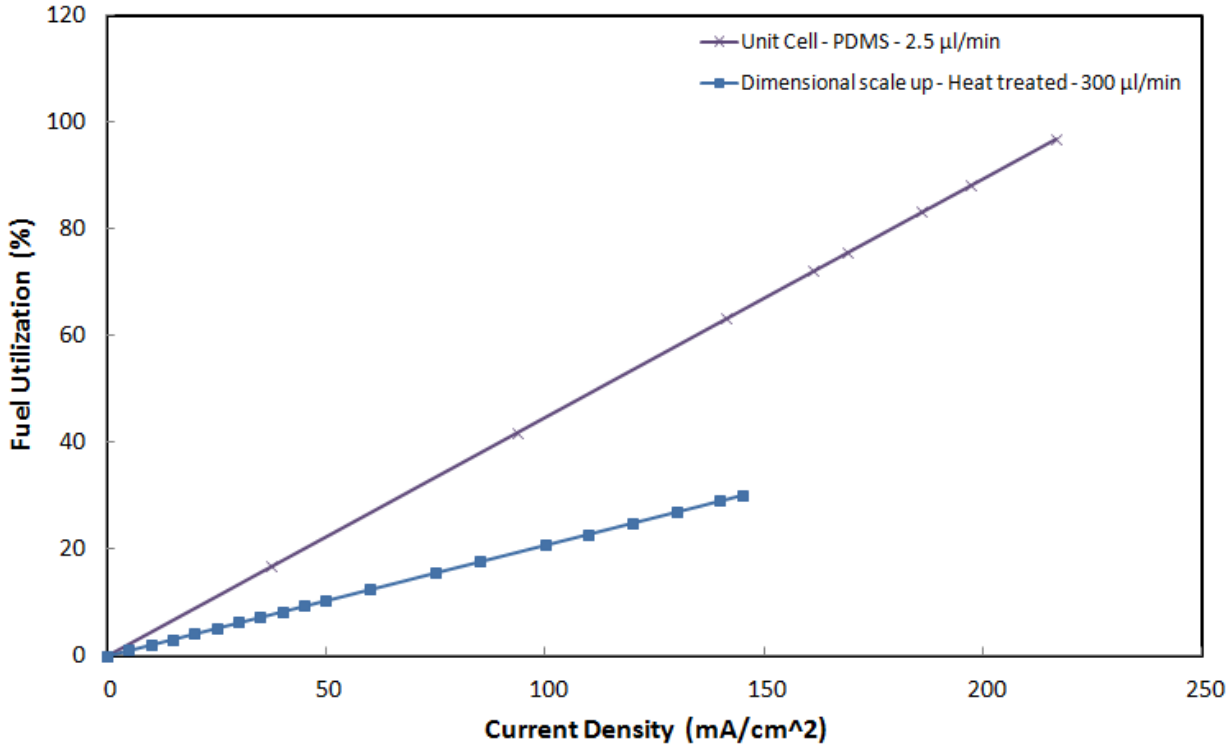

Figure 27: Dimensional scale up fuel utilization comparison

The reason of this performance discrepancy can be explained when we are looking at the fuel utilization profile (figure 27). When the fuel utilization reaches only 30% for the dimensional scale up, it is doubled (63%) at the same operating point for the unit cell.

At a larger scale, the manufacturing quality is not as precise and accurate as at a micro scale. Hence, flow shortcuts such as flow over and under the electrodes might also happen. With an active area of 2 cm² and a waste channel of 1 mm, the gravitational forces might be significant enough to disturb the co-laminar microfluidic flow, creating some cross over losses and possible discontinuities in the waste channel flow, resulting in reduced performance and operational stability of the cell and possibly increased ionic resistance.

6. CONCLUSIONS AND RECOMMENDATIONS

Avoiding the use of a membrane and catalyst, the two main causes of cost and failure in fuel cells, is a real challenge. Microfluidic fuel cells are promising contenders in terms of achieving useful performance levels for commercial applications while competing aggressively in terms of cost on a commercial scale.

In this work, multiplexing was successfully accomplished. We obtained twice the power output of the unit cell while managing to have a uniform reactant distribution and reach an equal flow sharing for both unit cells composing the array.

Dimensional scale up was also successfully accomplished. The main challenge of keeping a co-laminar microfluidic flow was accomplished on a much larger scale, up to two orders of magnitude larger than previously published devices, achieving a peak power of 130 mW.

Combining both solutions together is the key to a commercial product and the present work provides essential insight into the design of a commercial scale prototype. Many additional improvements are however possible in terms of design, manufacturing quality, material choice and possibly different fuel and oxidant.

With systematic CFD modeling studies, the channel design can be improved further and more novel reactant feeding designs can be evaluated to be able to multiplex more than 2 cells together. Cell design parameters such as electrode thicknesses ought to be optimized and check valves may be evaluated in order to balance the reactant flow to each cell, simplifying the design of the channels if needed. Moreover, the multiplexing scale up can be done by symmetry around the x axis and y axis in a simple way, multiplying by four the number of cells that we can possibly put together with an equal flow sharing. Increasing the electrode thickness or using check valves are definitely options to be considered in order to obtain a balanced flow sharing for each cell while keeping the channel design simple.

Several manufacturing processes, that are all compatible with high volume production have been investigated, improving the manufacturing quality, hence the performance,

after each iteration. When working with microfluidics and small scale fuel cells, the manufacturing quality is definitely an important factor that directly impacts the cell's performance. The PMMA patterning process is still under development and shows a much higher manufacturing quality over the two other manufacturing processes (laser etching PMMA and PDMS molding).

With the dimensional scale up, more materials can be investigated, and with better machining available, precision and accuracy can be improved. Even if the performance of the scaled up solutions are acceptable, when normalizing with the unit cell performance, there is still room for improvement. With absolute power peak above 130 mW, the dimensional scale up solution performance in terms of normalized power density and fuel utilization are still below the levels of the unit cell, meaning that there is still room to improve the dimensional scale up fuel cell.

The lower fuel utilization we obtained is definitely the main weakness of the dimensional scale up. As the dimensions are two orders of magnitude higher, the flow rate must be much higher, which can decrease the residence time. Finding a new electrode material with a higher contact surface area can be a way to improve the efficiency of the electrode. But the fuel utilization can also be significantly improved by finding the right trade off between the flow rate (increasing the residence time or lowering the reactants flow rate), the power and the size of such a microfluidic fuel cell device.

An EIS (Eletrochemical Impedance Spectrometry) study can be performed to help identify losses during when fuel cells are operating and help focus on the areas that need to be improved in the fuel cell.

REFERENCES AND CONTRIBUTION

[1] Larminie J., Dicks A., Fuel Cell Systems Explained, Second Edition, Wiley, England, 2003.

[2] http://www.fueleconomy.gov/feg/fcv_pem.shtml

[3] Tada T., Toshima N., Yamamoto Y., Inoue M., Investigation of catalyst degradation after single cell life tests, Electrochemistry -Tokyo-, 2007, 75 (2), 221-230.

[4] Kjeang E., Djilali N., Sinton D., Microfluidic fuel cells: A review, Journal of Power Sources, 2009, 186, 353-369.

[5]Bullen R.A., Arnot T.C., Lakeman J.B., Walsh F.C., Biofuel cells and their development, Biosensors and Biomechanics, 2006, 21, 2015-2045.

[6] Wang H., Bernarda A., Huang C., Lee D.J., et al., Micro-sized microbial fuel cell: A mini review, Biosource Technology, 2011, 102, 235-243.

[7] Lee J., Kjeang E., A perspective on microfluidic biofuel cells, Biomicrofluidics, 2010, 4(041301).

[8] Ho B., Kjeang E., Microfluidic fuel cell systems, Central European Journal of Engineering, 2011, 1, 123-131.

[9] Brushett F., Zhou W., Jayashree R., Kennis P., Alkaline microfluidic hydrogen-oxygen fuel cell as a cathode characterization platform, Journal of Electrochemical Society, 2009, 156(5), B565-B571.

[10] Naughton M., Brushett F., Kenis P., Carbonate resilience of flowing electrolyte-based alkaline fuel cells, Journal of Power Sources, 2011, 196, 1762-1768.

[11] Gago A., Morales-Acosta D., Arriaga L., Alonso-Vante N., Carbon supported ruthenium chalogenide as cathode catalyst in a microfluidic formic acid fuel cell, Journal of Power Sources, 2011, 196, 1324-1328.

[12] Morales-Acosta D., Rodriguez H., Godinez L. Arriaga L.G., Performance increase of microfluidic formic acid fuel cell using Pd/MWCNTs as catalyst, Journal of Power Sources, 2010, 195, 1862-1865.

[13] Hollinger A., Maloney R., Jayashree R. Natarajan D., et al. Nanoporous separator and low fuel concentration to minimize crossover in direct methanol laminar flow fuel cell, Journal of Power Sources, 2010, 195, 3523-3528.

[14] Whipple D., Jayashree R., Egas D., Alonso-Vante N., et al, Ruthenium cluster-like chalogenide as a methanol tolerant cathode catalyst in air-breathing laminar flow fuel cells, Electrochimica Acta, 2009, 54, 4384-4388.

[15] Salloum K., Posner J., Counter flow membraneless microfluidic fuel cell, Journal of Power Sources, 2010, 195, 6941-6944.

[16] Salloum K, Posner J., A membraneless microfluidic fuel cell stack, Journal of Power Pources, 2011, 196, 1229-1234.

[17] Hao Yu E., Krewer U., Scott K., Principes and materials aspects of direct alkaline alcohol fuel cell, Energies, 2010, 3, 1499-1528.

[18] Gulzow E., Schule M., Long-term operation of AFC electrodes with CO2 containing gases, Journal of Power Sources, 2004, 127, 243-251.

[19] S. Supramaniam, Fuel Cells: From Fundamentals to Applications, Springer, New York, 2006.

[20] Viscosity of aqueous KOH solutions, 2010. Retrieved from http://koh.olinchloralkali.com/TechnicalInformation/KOH%20Viscosity.pdf.

[21] Alcaide F., Brillas E., Cabot P.L., Hydrogen oxidation reaction in a Pt-catalyzed gas diffusion electrode in alkaline medium, Journal of Electrochemical Society, 2005, 152, E319–E327.

[22] Kjeang E., Brolo A.G., Harrington D.A., Djilali N., et al.., Hydrogen Peroxide as an Oxidant for Microfluidic Fuel Cells, Journal of the Electrochemical Society, 2007, 154, B1220-B1226

[23] Kjeang E., Michel R., Harrington D.A., Sinton D., et al., An Alkaline microfluidic fuel cell based on formate and hypochlorite bleach, Electrochimica Acta, 2008, 54, 698-705.

[24] United States Patent Application #20090023036.

[25] Jayashree R.S., Gancs L., Choban E.R., Primak A., et al., Air-breathing laminar flow-based microfluidic fuel cell, Journal of American Chemical Society, 2005, 127, 16758-16759.

[26] Jayashree R.S., Egas D., Spendelow J.S., Natarajan D., et al, Air-breathing laminar flow based direct methanol fuel cell with alkaline electrolyte, Electrochemical and Solid-State Letters, 2006, 9(5), A252-A256.

[27] Shyu J., Wei C., Lee C., Wang C., Investigation of bubble effect in microfluidic fuel cell by a simplified microfluidic reactor, Applied Thermal Engineering, 2010, 30, 1863-1871.

[28] Fu B., Pan C., Simple channel geometry for enhancement of chemical reactions in microchannels, Industrial and Engineering Chemistry Research, 2010, 49, 9413-9422.

[29] Cohen J.L., Volpe D.J., Daron A.W., Pechenik A., et al., A dual electrolyte H2/O2 planar membraneless microchannel fuel cell system with open circuit potentials in excess of 1.4V, Langmuir, 2005, 21, 3544-3550.

[30] Mutolo P.F., the PM2TM power cell: planar, membraneless microfluidic portable power, Proceedings of 11th Annual International Conference on Small Fuel Cells 2009, May 7-8, 2009, Orlando, FL, USA.

[31] D'Couto C., High power density liquid fuel cells based on porous silicon for portable power application in air free and air quality limited environments, Proceedings of 11th Annual International Conference on Small Fuel Cells 2009, May 7-8, 2009, Orlando, FL, USA.

[32] Ferrigno R., Stroock A.D., Clark T.D., Mayer M., et al., Membraneless vanadium redox fuel cell using laminar flow, 2002, Journal of American Chemical Society, 124, 12930-12931.

[33] Kjeang E., McKechnie J., Djilali N., Sinton D., Planar and Three-Dimensional Microfluidic Fuel Cell Architectures Based on Graphite Rod Electrodes, Journal of Power Sources, 2007, 168, 379-390.

[34] Kjeang E., Proctor B.T., Brolo A.G., Harrington D.A., et al., High-Performance Microfluidic Vanadium Redox Fuel Cell, Electrochimica Acta, 2007, 52, 4942-4946.

[35] Kjeang E., Michel R., Harrington D.A., Djilali N., et al., A Microfluidic Fuel Cell with Flow-Through Porous Electrodes, Journal of the American Chemical Society, 2008, 130, 4000-4006.

[36] Moore S., Sinton D., Erickson D., A plate-frame flow-through microfluidic fuel cell stack, Journal of Power Sources, 2011, 196, 9681-9487.

[37] Haiducu M., Rahbar M., Foulds I.G., Johnstone R.W., et al., Deep-UV patterning of commercial grade PMMA for low-cost, large-scale microfluidics, Journal of Micromechanics and Microengineering, 2008, 18 (11), 115029

[38] Haiducu M., Sameoto D., Foulds I., Johnstone R.W., et al., Bosch-like method for creating high aspect ratio poly(methyl methacrylate) (PMMA) structures, Proceedings of SPIE Photonics West, 8248, San Francisco, 2012.

[39] I. S. Hussaini and C. Y. Wang, Measurement of Relative Permeability of Fuel Cell Diffusion Media, Journal of Power Sources, 2010, 195, 3830-3840.

[40] White F.M., Fluid Mechanics, Fifth edition, Mc Graw Hill, New York, 2003.

[41] C. Blanc, A. Rufer, Understanding the Vanadium Redox Flow Batteries, Laboratoire d'Electronique Industrielle, Ecole Polytechnique Federale de Lausanne, Switzerland.

[42] J. Hong, Electrochemical analysis of vanadium redox reactions on porous carbon electrodes, Simon Fraser University, 2011.